

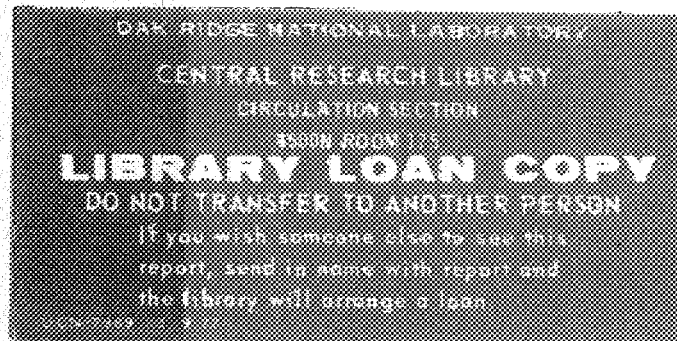
ORNL/TM-11026

OAK RIDGE
NATIONAL
LABORATORY

MARTIN MARIETTA

Two Dimensional Maps Generated by Competitive Systems

Y. Y. Azmy
V. Protopopescu



OPERATED BY
MARTIN MARIETTA ENERGY SYSTEMS, INC.
FOR THE UNITED STATES
DEPARTMENT OF ENERGY

Printed in the United States of America. Available from
National Technical Information Service
U.S. Department of Commerce
5285 Port Royal Road, Springfield, Virginia 22161
NTIS price codes--Printed Copy: A03; Microfiche A01

This report was prepared as an account of work sponsored by an agency of the United States Government. Neither the United States Government nor any agency thereof, nor any of their employees, makes any warranty, express or implied, or assumes any legal liability or responsibility for the accuracy, completeness, or usefulness of any information, apparatus, product, or process disclosed, or represents that its use would not infringe privately owned rights. Reference herein to any specific commercial product, process, or service by trade name, trademark, manufacturer, or otherwise, does not necessarily constitute or imply its endorsement, recommendation, or favoring by the United States Government or any agency thereof. The views and opinions of authors expressed herein do not necessarily state or reflect those of the United States Government or any agency thereof.

ORNL/TM-11026

Engineering Physics and Mathematics

**Two Dimensional Maps Generated
by Competitive Systems**

Y. Y. Azmy and V. Protopopescu

Date Published - February 1989

NOTICE: This document contains information of a preliminary nature. It is subject to revision or correction and therefore does not represent a final report.

Prepared by the
OAK RIDGE NATIONAL LABORATORY
Oak Ridge, Tennessee 37831
operated by
MARTIN MARIETTA ENERGY SYSTEMS, INC.
for the
U.S. DEPARTMENT OF ENERGY
under contract DE-AC05-84OR21400



3 4456 0284644 6

CONTENTS

ABSTRACT	v
1. INTRODUCTION	1
2. DERIVATION OF THE ONE-DIMENSIONAL, DISCRETE-VARIABLE COMBAT MODEL	5
3. EFFECT OF CONVECTION ON THE ONE-SPECIES SYSTEM	9
3.1 FIXED POINTS	9
3.2 PERIODIC SOLUTIONS	18
3.3 NON-VANISHING CONVECTION	25
4. THE DYNAMICS OF INTERACTING TWO-SPECIES SYSTEMS	30
REFERENCES	33

LIST OF FIGURES

Figure		Page
1	The phase portrait for the system of ODE's, Equations (1.3) with $\gamma = .5$: $\bullet \equiv$ fixed point, $\rightarrow \equiv$ direction of flow for increasing time	2
2	Classes of fixed point solutions to the nonconvective one-dimensional case ignoring the effect of the boundary condition at $x = L, m = M$	12
3	Bifurcation diagram for the $\lambda = 2\delta$ fixed points (solid line) and the $\lambda = 3\delta$ fixed points (dashed line)	14
4	Bifurcation diagram for the $\lambda = 4\delta$ fixed points	16
5	Bifurcation of one $\lambda = 4\delta$ fixed point, the (f_3, f_6, f_4, f_6) sequence from the positive branch of the $\lambda = 2\delta$ fixed point	17
6	Sample period-2 solution for $0 \leq m \leq 50, \alpha = 16.8, D = .002$, and initial condition $u^{0,0} = 3.1/3, u^{0,m} = 0, m > 0$	20
7	Region of existence of the period-2 second class solution in the (\mathcal{K}, ζ) plane. The part of this region that is physically acceptable, $\mathcal{K}, \zeta \geq 0$, is hatched	22
8	Bifurcation diagram for period-2 first class (dashed) and second class (solid) solutions as a function of ζ for various values of \mathcal{K}	23
9	Bifurcation diagram for period-2 second class solution as a function of \mathcal{K} for various values of ζ	24
10	Sample plots of u vs. x at two consecutive time steps, with parameter values corresponding to points surrounding discontinuities in Figure 4 of Ref. 12. These plots clearly show that these discontinuities occur at parameter values that cause a change in the solution class (i.e., the symmetry relations at the left boundary)	26

ABSTRACT

By discretizing time and space in a PDE model for competitive systems, we derive the corresponding discrete maps. We analyze these maps from an analytical and numerical viewpoint with emphasis on the military interpretation of the system. For the one-species map we study the effect of convection on the bifurcation behavior and we find periodic solutions. For the two-species map, we limit our analysis to an illustrative example, but we indicate the general procedure.

1. INTRODUCTION

One of the most common methods for the numerical solution of ordinary differential equations (ODE's) is to transform the continuum system, through some approximation procedure, into a set of discrete-variable, algebraic equations. The fundamental assumption in such a situation is that the solution to the approximate difference equations converges to the solution of the original ODE as the number of discrete variables representing the continuum variables approaches infinity. When this is indeed the case, one can estimate the range of deviation of the solution to the ODE's from the calculated discrete-variable solution through a theoretical or empirical error analysis, thus determining the degree of confidence one can have in the numerical solution. However, simple examples relevant to combat modeling exist where the above assumption fails so severely that the numerical solution may violate certain properties that are essential for the physical acceptability of the solution, such as, for instance, positivity.

To set the matter in perspective, let us start with an example, namely, the two-species, Lotka-Volterra competitive system described by the ODE system

$$du_i/dt = u_i(\alpha_i - \beta_i u_j), \quad i, j = 1, 2, \quad j \neq i, \quad \alpha_i, \beta_i > 0. \quad (1.1)$$

Introducing the scaled variables,

$$\begin{aligned} v_i &\equiv (\beta_j/\alpha_j)u_i, \quad i, j = 1, 2, \quad i \neq j, \\ T &\equiv \alpha_1 t, \quad \gamma \equiv \alpha_2/\alpha_1 > 0, \end{aligned} \quad (1.2)$$

the system of Equations (1.1) becomes,

$$\begin{aligned} dv_1/dT &= v_1(1 - v_2), \\ dv_2/dT &= \gamma v_2(1 - v_1). \end{aligned} \quad (1.3)$$

Solutions to this system have the following properties,

- i. The solution $v_i(T)$, hence also $u_i(T)$, is positive.
- ii. There are two fixed points at $V_0 \equiv (v_1 = 0, v_2 = 0)$ and $V_1 \equiv (v_1 = 1, v_2 = 1)$.
- iii. V_0 is unstable.
- iv. V_1 is a saddle point.

These properties are schematically represented in the phase portrait in Figure 1, which represents the solution to Equations (1.3), namely,

$$v_2 e^{-v_2} = c [v_1 e^{-v_1}]^\gamma. \quad (1.4)$$

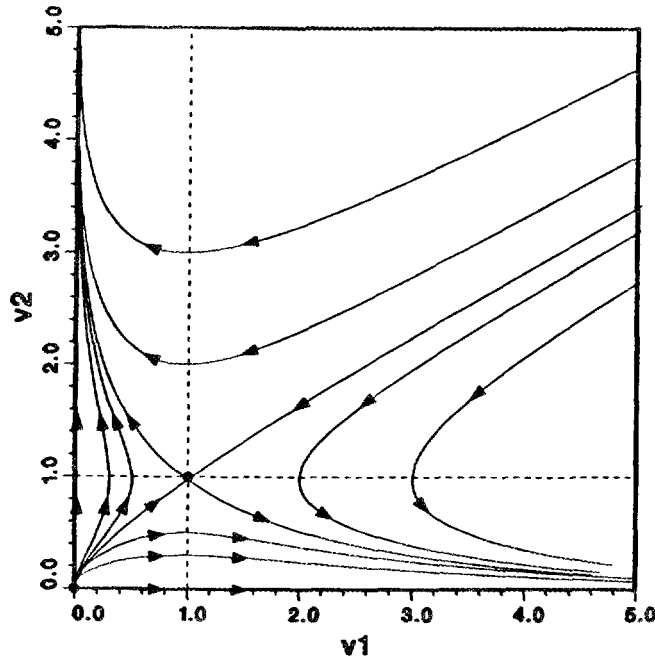


Figure 1. The phase portrait for the system of ODE's, Equations (1.3) with $\gamma = .5$: $\bullet \equiv$ fixed point, $\rightarrow \equiv$ direction of flow for increasing time.

By applying the explicit finite difference approximation, to Equations (1.3) we obtain,

$$\begin{aligned} v_1^{n+1} &= v_1^n + \tau v_1^n (1 - v_2^n), \\ v_2^{n+1} &= v_2^n + \tau \gamma v_2^n (1 - v_1^n), \quad n > 0. \end{aligned} \quad (1.5)$$

In Equations (1.5), we assumed that the time variable has been divided into equal intervals of size τ , so that $T_n = n\tau$, and $v_i^n = v_i(T_n)$, $i = 1, 2$. It follows immediately that if for some n , including the initial guess $n = 0$, either $v_2^n > 1 + 1/\tau$ and $v_1^n > 0$, or $v_1^n > 1 + 1/\gamma\tau$ and $v_2^n > 0$, then $v_1^{n+1} < 0$, or $v_2^{n+1} < 0$, respectively, so that the invariance of the positive quadrant of the phase plane is not preserved by such numerical solutions. Moreover, the unbounded nature of all the trajectories but two in the phase plane of the continuum system, Figure 1, means that if the numerical solution resembles this feature, then no matter how small we choose the time step τ , either v_1^n or v_2^n will become large enough that v_2^{n+1} or v_1^{n+1} will become negative, respectively.

On the other hand, the implicit variant of the finite difference method, applied to Equations (1.3), results in

$$\begin{aligned} v_1^{n+1} &= v_1^n + \tau v_1^{n+1}(1 - v_2^{n+1}), \\ v_2^{n+1} &= v_2^n + \gamma\tau v_2^{n+1}(1 - v_1^{n+1}). \end{aligned} \quad (1.6)$$

Solving these two equations simultaneously for v_i^{n+1} yields,

$$\begin{aligned} v_1^{n+1} &= \frac{1}{2} \left\{ - \left[\frac{v_2^n - \gamma v_1^n}{\gamma(1-\tau)} + \frac{1-\gamma\tau}{\gamma\tau} \right] \pm \sqrt{ \left\{ \frac{v_2^n - \gamma v_1^n}{\gamma(1-\tau)} + \frac{1-\gamma\tau}{\gamma\tau} \right\}^2 + \frac{4(1-\gamma\tau)v_1^n}{\gamma\delta(1-\tau)} } \right\}, \\ v_2^{n+1} &= \frac{1}{2} \left\{ - \left[\frac{\gamma v_1^n - v_2^n}{1-\gamma\tau} + \frac{1-\tau}{\tau} \right] \pm \sqrt{ \left\{ \frac{\gamma v_1^n - v_2^n}{1-\gamma\tau} + \frac{1-\tau}{\tau} \right\}^2 + \frac{4(1-\tau)v_2^n}{\tau(1-\gamma\tau)} } \right\}. \end{aligned} \quad (1.7)$$

If the terms in the square brackets on the RHS's of Equations (1.7) are negative, then there is at least one positive solution. Otherwise, we must choose the step size τ so that $1 - \tau$ and $1 - \gamma\tau$ have the same sign; that is, the condition

$$\begin{aligned} \tau &< \frac{1}{\gamma} < 1, \quad \text{if } \gamma > 1, \\ \tau &> \frac{1}{\gamma} > 1, \quad \text{if } \gamma < 1, \end{aligned} \quad (1.8)$$

is sufficient (but not necessary) to preserve the invariance of the positive quadrant of the phase plane.

It is also possible for Equations (1.5), obtained with the explicit method to produce periodic solutions, even though the ODE system does not. This is done by calculating v_i^{n+2} from Equations (1.5) and setting them equal to v_i^n , then solving for the latter. When this is done, we obtain the condition,

$$\tau < 2/\sqrt{\gamma}, \quad (1.9)$$

that the step size has to satisfy in order to avoid periodic solutions to the explicit method.

So, it is clear that studying the dynamics of continuum systems using discrete-variable approximations can be very misleading unless great caution is exercised. On the other hand, iterative maps of the type discussed above are interesting in their own right as they can be used to model certain phenomena in which states evolve in a discrete, rather than continuous, manner. The most successful such example is the predator-prey system¹⁾ where one looks at the evolution of generations of the two species and ignores the details of the inter-generation evolution. The same argument may be applied to the case of combat in which the dynamic evolution of the war depends very strongly on the individual outcome of many battles, and very weakly on the details of each battle. Also, the same logic can be applied on various scales to the various size units in the military structures. The finest such scale, for example, would be the temporal development of a single battle where only the final result of a one-on-one confrontation between two soldiers, tanks, fighters, etc., is important, while the details of obtaining this result are far less relevant.

The approach we take in this work is to derive an iterative map, through the finite difference approximation, from a combat model based on a system of coupled nonlinear partial differential equations (PDE) in one spatial dimension, with diffusion and convection.²⁾ This is done in Section 2. However, we do not give any importance to the approximate correspondence between the difference and differential sets of equations; rather, we study the dynamics of the difference equations by themselves for the reasons discussed above, without investigating at this stage the convergence to the solution of the PDE system. In Section 3, we review previous work on the one species system, and discuss the observed effect of convection on the bifurcation diagram and on the dynamics as a whole. Section 4 contains the results of our investigation into the two-species system, with samples of battle scenarios.

2. DERIVATION OF THE ONE-DIMENSIONAL, DISCRETE-VARIABLE COMBAT MODEL

Analytic models for combat (competition) originate in the seminal paper by Lanchester³⁾ who described the dynamics of fighting troops in the battlefield by simple nonlinear ODE's. Two basic models were proposed to account for aimed and area fire, and were supposed to support his principle of concentration. A good review on Lanchester's equations and later development can be found in Taylor's monograph.⁴⁾

One of the major drawbacks of the competition/combat models based on ODE's is that they do not account for spatial dependence in the absence of which movement, expansion, advance, retreat, maneuvers, and deployment, cannot be properly described.

To correct—at least in part—this deficiency, an analytic description of low intensity combat based on semilinear parabolic PDE's has been recently proposed.⁵⁾ A typical example for two species reads:

$$\frac{\partial u_i(x, t)}{\partial t} = \frac{\partial}{\partial x} \left[D_i(x) \frac{\partial u_i}{\partial x} \right] - \frac{\partial}{\partial x} [c_i(x)u_i] - \sum_{j,k=1}^2 [\alpha_{ijk}u_ju_k - \beta_{ij}u_j] + s_i(x), \quad t > 0, \quad x \in (0, L), \quad (2.1)$$

with initial conditions

$$u_i(x, 0) = u_i^{(0)}(x) \quad (2.2)$$

and boundary conditions of mixed type,

$$a_i^k \frac{\partial}{\partial x} u_i(x_i^k, t) + b_i^k u_i(x_i^k, t) = e_i^k, \quad i, k = 1, 2. \quad (2.3)$$

In general, a_i^k , b_i^k , and e_i^k are functions of x and t but in the present work, they are considered constant for simplicity. The two points x_i^k , $k = 1, 2$ are noncoincident in general, but if they are, then it must be required that the two equations (2.3) are compatible and linearly independent for each species.

In the evolution Equations (2.1), the different terms have the following interpretations:

- i) $\frac{\partial}{\partial x} [D_i(x) \frac{\partial u_i}{\partial x}]$ is a (Fickian) diffusion term that models that natural tendency of any distribution to lose its initial configuration. The small scale irregular diffusive movement is produced by stochastic causes.
- ii) $\frac{\partial}{\partial x} [c_i(x)u_i]$ describes the large scale, ordered flow through convection. It captures the intentional character of the directed movement as opposed to the random character of the diffusive displacement.
- iii) The interaction terms under the sum describe re-supply, self-repressing effects, and attrition while the terms $s_i(x)$ model external sources.

In general, systems of the type (2.1)–(2.3) (usually called reaction-diffusion (R–D) systems) appear quite naturally in biology and ecology,⁶⁾ as well as in chemistry, metallurgy, fluid flow through porous media, etc. Recent summaries of theoretical, applied, and computational aspects of R–D systems can be found in the monographs of Fife,⁷⁾ Smoller,⁸⁾ and Oran and Boris.⁹⁾ In the following, we shall study the system (2.1)–(2.3) from a different viewpoint, namely, we shall transfer it into a map. The possible interest in this approach was suggested by (i) the potential elements of order and chaos contained in the R–D systems; (ii) the stability-instability interplay of numerical schemes used to solve PDE's, (iii) the principal resemblance of these schemes with discrete maps, (iv) the potential for order and chaos in discrete maps, (v) the extreme sensitivity of the solutions of certain R–D systems to minute changes in interactions, boundary conditions (B.C.), dimension and even form of phase space, (vi) predictability and unpredictability issues, (vii) the discrete nature of combat, and (viii) potentials of cellular automata. In short, a discretized version of the PDE (2.1) can be viewed either as a simplified version of the PDE system (2.1)–(2.3) or as a model in itself that could be derived, in principle, from the very beginning. In fact, further studies will reveal whether the discrete version is not a better approximation of the competitive systems than the continuous system. At this point, we shall view it as a promising alternative to the continuous R–D type model recently proposed to describe low intensity combat.^{5,10,11)}

We divide the time-space plane into closed rectangular regions of equal size, and we denote the time step τ and the spatial cell size by δ . That is, the point of intersection of the n th temporal line and the m th spatial line, denoted (n, m) , represents time level $t_n = n\tau$ at the point $x_m = m\delta$ in the physical space; $L = x_M = M\delta$. The density of species i at point (n, m) is denoted $u_i^{n,m}$, while volumetric quantities, such as the diffusion coefficient, the convection speed, and the external source are constant with respect to time, and piecewise constant within the spatial cell bounded by x_{m-1} and x_m , and are denoted D_i^m , c_i^m , and s_i^m , respectively, for species $i = 1, 2$. The quadratic and linear interaction coefficients, α_{ijk} and β_{ij} , respectively, are constant with respect to both time and space. Now, we apply an explicit (first order) finite difference approximation²⁾ to the time derivatives, a space-centered (second order) finite difference approximation²⁾ to the diffusion terms, and an upwind finite difference approximation²⁾ to the convective terms to obtain the difference equations:

$$\begin{aligned} \left[\frac{u_i^{n+1,m} - u_i^{n,m}}{\tau} \right] &= \left[\frac{D_i^{m+1}(u_i^{n,m+1} - u_i^{n,m}) - D_i^m(u_i^{n,m} - u_i^{n,m-1})}{\delta^2} \right] \\ &- (1 - w_i^{m+1})c_i^{m+1} \left[\frac{u_i^{n,m+1} - u_i^{n,m}}{\delta} \right] - w_i^m c_i^m \left[\frac{u_i^{n,m} - u_i^{n,m-1}}{\delta} \right] \\ &- \sum_{j,k=1}^2 [\alpha_{ijk} u_j^{n,m} u_k^{n,m} + \beta_{ij} u_j^{n,m}] + \left[\frac{s_i^m + s_i^{m+1}}{2} \right], \quad i = 1, 2. \end{aligned} \tag{2.4}$$

In Equation (2.4), w_i^m is the ‘‘upwind parameter’’ which takes the value 0(1) if c_i^m is negative (positive), in order to enforce the unconditionally stable²⁾ upwind differencing of the convection terms. To simplify the writing, we shall define

$$\begin{aligned} \mathcal{D}_{i+}^m &\equiv \frac{D_i^{m+1}}{\delta^2} - (1 - w_i^m) \frac{c_i^{m+1}}{\delta} . \\ \mathcal{D}_{i-}^m &\equiv \frac{D_i^m}{\delta^2} + \frac{w_i^m c_i^m}{\delta} , \\ \mathcal{D}_i^m &\equiv \frac{1}{\tau} - \mathcal{D}_{i+}^m - \mathcal{D}_{i-}^m , \end{aligned} \quad (2.5)$$

so that Equations (2.4) take the multicomponent iterative map structure,

$$\begin{aligned} u_i^{n+1,m} = \tau &\left\{ \mathcal{D}_{i+}^m u_i^{n,m+1} + \mathcal{D}_i^m u_i^{n,m} + \mathcal{D}_{i-}^m u_i^{n,m-1} \right. \\ &\left. - \sum_{j,k=1}^2 \alpha_{ijk} u_j^{n,m} u_k^{n,m} - \sum_{j=1}^2 \beta_{ij} u_j^{n,m} + \bar{s}_i^m \right\} , \\ &i = 1, 2, \quad n \geq 0, \quad 0 \leq m \leq M . \end{aligned} \quad (2.6)$$

To discretize the boundary condition, Equation (2.3) at point $x_i^k = x_{m_k} = m_k \delta$, for some $0 \leq m_k \leq M$, we note that a_i^k and b_i^k cannot vanish simultaneously. Therefore, if $a_i^k = 0$, the boundary condition reduces to

$$u_i^{n,m_k} = e_i^k / b_i^k , \quad b_i^k \neq 0, \quad n > 0 . \quad (2.7)$$

The general case $a_i^k, b_i^k \neq 0$ includes as a special case $a_i^k \neq 0, b_i^k = 0$. If the point x_i^k is an internal point, i.e., $0 < m_k < M$, then the first order derivative in Equation (2.3) is immediately discretized using the same space-centered approximation which was applied in the derivation of Equation (2.4) above. This case is not of interest and will not be considered further. If x_i^k is truly a boundary point, $m_k = 0$, for example, then applying the space-centered approximation to Equation (2.3) yields

$$\frac{a_i^k}{2\delta} [u_i^{n,1} - u_i^{n,-1}] + b_i^k u_i^{n,0} = e_i^k . \quad (2.8)$$

This equation is solved for the fictitious quantity $u^{n,-1}$ (note that $a_i^k \neq 0$), then it is used together with $u_i^{n,0}$ and $u_i^{n,1}$ in Equation (2.6) to calculate $u_i^{n+1,0}$, assuming that the properties of the fictitious computational cell $m = 0, x \in [-\delta, 0]$, are identical to those of the adjacent computational cell $m = 1$. The boundary condition at $x = L$ is treated in an analogous way.

Given an initial condition of the form $u^{0,m}, m = 0, \dots, M$, Equation (2.6) and the appropriate set of discrete-variable boundary conditions represent an iterative map where n , the time step index plays the role of the iteration index. At each time

step, the state of the system, $u_i^{n,m}$, is fully determined by the map from the previous state $u_i^{n-1,m}$. The iterative map can have one or more fixed points, periodic states which may undergo period doubling bifurcations, and transition to chaos, depending on the specific set of parameters used in a given case. The determination of the various possible asymptotic states, their stability, basins of attraction, and their bifurcation into other states, and particularly understanding the dependence of all these things on the various parameters involved in the system is of great importance. For example, in combat modeling, two asymptotic states may exist, one representing victory and the other defeat for a given army. Knowledge of the dependence of the dynamics of the model on the system parameters should allow the commander of this army to control these parameters in order to bias the battle outcome in his army's favor.

We implemented the iterative map for the one-dimensional two-species system described above into the computer code CMAP1. The code accepts boundary conditions of the mixed type specified at $x = 0$ and $x = L$ for each species. The initial condition can be uniformly specified in the input file, or read-in from another file to enable continuation of a previous calculation. All the parameters in the system are specified in the input, except for the number of species which is "hardwired" to two. Several options exist for handling the output data: it can either be printed out in an output file, or it can be used in conjunction with DISPLA graphics routines to generate time evolution plots of each species density on one of the boundaries, or to animate the time evolution of the densities of the two species simultaneously as a function of space. The first option is useful in comparing numbers exactly to determine convergence to a fixed point or to a periodic state. The second option was used to compare our results with previous work as described in the next section, and the third mode, animation in time, is particularly useful in gaining a comprehensive feeling for the extremely large amount of data generated, which can guide the intuition in probing complex dynamical patterns. In addition, minor modifications can be made to the coding of these three options, for example, to obtain "snap shots" of the evolution.

One of the interesting features of the iterative map approach to solving this system is that it is highly parallelizable. Equation (2.6) and the boundary conditions relate only three spatial points, at most, at the old time level to one species' density at the new time level. Hence, by decomposing the spatial mesh into sets of adjacent, non-intersecting regions, the only connection between the computational development in one region and a neighboring region will be the mesh point on the common boundary. That is, each region can be assigned to one processor which calculates $u_i^{n+1,m}$ for all interior points from $u_i^{n,m}$ and shares with other CPU's only the species density on the common inter-region boundaries. It is not realistic to expect very high efficiencies from the parallelization in the one-dimensional case, because the interprocessor communication overhead will probably be comparable to the solution time on each processor. However, two- and three-dimensional extensions of the present work will be very suitable for implementation on parallel machines, and efficiencies in excess of 80%, with about ten-fold speedups, especially on shared memory machines, are conceivable.

3. EFFECT OF CONVECTION ON THE ONE-SPECIES SYSTEM

The one-species system equations can be obtained from the equations of Section 2 by setting

$$\alpha_{ijk} = \beta_{ij} = 0, \text{ if } i \neq j \text{ or } k. \quad (3.1)$$

This results in two non-interacting species. Substituting Equation (3.1) into Equations (2.6) yields the iterative map

$$\begin{aligned} u_i^{n+1,m} = & \tau \{ \mathcal{D}_{i+}^m u_i^{n,m+1} + \mathcal{D}_i^m u_i^{n,m} + \mathcal{D}_{i-}^m u_i^{n,m-1} \\ & - \alpha_i (u_i^{n,m})^2 - \beta_i u_i^{n,m} + \bar{s}_i^m \}, \quad i = 1, 2, \end{aligned} \quad (3.2)$$

which is supplemented by appropriate discrete-variable boundary conditions and solved using the computer program described in the previous section. Indeed, the coding of the program was benchmarked for several dynamic regimes against the results of Mitchell and Bruch¹²⁾ for a one-species non-convective system. In this section, we review previous work^{12,13)} on this system and expand on the available description of its dynamics, then proceed to investigate the effect of convection on the dynamics.

Consider the non-convective one-species system described by

$$\begin{aligned} u^{n+1,m} = & u^{n,m} + \frac{\tau D}{\delta^2} [u^{n,m+1} - 2u^{n,m} + u^{n,m-1}] + \tau \alpha u^{n,m} [1 - u^{n,m}], \\ & n > 0, \quad 0 < m < M, \\ u^{0,0} = & U, \quad u^{0,m} = 0, \quad m > 0, \\ u^{n,M} = & 0, \quad u^{n+1,0} = u^{n,0} + \frac{2D\tau}{\delta^2} [u^{n,1} - u^{n,0}] + \tau \alpha u^{n,0} [1 - u^{n,0}], \end{aligned} \quad (3.3)$$

which follows directly from Equation (3.2) and the boundary conditions if we drop the species index, set the external source and convection equal to zero, and set $\alpha = \beta_i = -\alpha_i$. This system was studied in Refs. 12 and 13, but the results were limited to experimentation with the dynamics of this system as a function of the various parameters. That is, a number of asymptotic states were obtained^{12,13)} from a given initial condition without relating them to one another in a comprehensive way. Moreover, the results presented in these previous studies were extracted from the behavior of only one variable, namely $u^{n,0}$, under the mapping described by Equations (3.3). This resulted in confusing solution branches^{12,13)} with one another as described below. In contrast, here we consider the dynamics of the M discrete-variables, $u^{n,m}$, $m = 0, \dots, M-1$, and we obtain some asymptotic states, i.e., $n \rightarrow \infty$, independent of the initial condition.

3.1 FIXED POINTS

A fixed point ${}^1u^m$ of the map, Equations (3.3), is defined by

$$\begin{aligned} \frac{D}{\delta^2} [{}^1u^{m+1} - 2{}^1u^m + {}^1u^{m-1}] + \alpha {}^1u^m [1 - {}^1u^m] &= 0, \quad 0 < m < M, \\ {}^1u^M &= 0, \quad \frac{2D}{\delta^2} [{}^1u^1 - {}^1u^0] + \alpha {}^1u^0 [1 - {}^1u^0] = 0. \end{aligned} \quad (3.4)$$

This can be reduced to a single equation of order 2^M in ${}^1u^0$ as follows. First, we solve the boundary condition at $m = 0$ for ${}^1u^1$,

$${}^1u^1 = {}^1u^0 \left[\left(1 - \frac{\alpha\delta^2}{2D} \right) + \frac{\alpha\delta^2}{2D} {}^1u^0 \right]. \quad (3.5)$$

Similarly, the map equation is solved at each point m for ${}^1u^{m+1}$ in terms of ${}^1u^m$ and ${}^1u^{m-1}$; i.e.,

$${}^1u^{m+1} = 2{}^1u^m \left[\left(1 - \frac{\alpha\delta^2}{2D} \right) + \frac{\alpha\delta^2}{2D} {}^1u^m \right] - {}^1u^{m-1}, \quad 1 \leq m < M - 1. \quad (3.6)$$

Starting at $m = 1$, the mesh is swept recursively in the direction of increasing m by eliminating ${}^1u^m$ and ${}^1u^{m-1}$ in terms of ${}^1u^0$ alone using expressions derived in previous steps of the sweep. Applying the boundary condition at $m = M - 1$,

$$2{}^1u^{M-1} \left[\left(1 - \frac{\alpha\delta^2}{2D} \right) + \frac{\alpha\delta^2}{2D} {}^1u^{M-1} \right] - {}^1u^{M-2} = 0, \quad (3.7)$$

(where ${}^1u^{M-1}$ and ${}^1u^{M-2}$ are actually expressed as polynomials in ${}^1u^0$ as described above) produces a single polynomial condition of order 2^M in ${}^1u^0$. Each homogeneous real root of this polynomial represents a fixed point of the map, where the remaining ${}^1u^m$, $0 < m < M$ can be calculated by substituting ${}^1u^0$ successively in Equations (3.5) and (3.6). Clearly, the number of fixed points of the map can become very large as M increases, making it practically impossible to explicitly calculate them all. One simple fixed point, the trivial solution ${}^1u^m = 0$, $0 \leq m \leq M$, follows directly from the homogeneity of the polynomial in ${}^1u^0$. Another approximate solution which has been obtained before^{12,13)} ignores the boundary condition at $m = M$ altogether, and assumes a uniform density distribution,

$${}^1u^0 = {}^1u^{m-1} = {}^1u^m = {}^1u^{m+1}, \quad m = 1, \dots, M - 1. \quad (3.8)$$

Substituting Equation (3.8) into (3.5) and (3.6) immediately results in the trivial fixed point, and

$${}^1u^m = 1, \quad m = 0, \dots, M. \quad (3.9)$$

This fixed point is only approximate because it does not satisfy the boundary condition, Equation (3.7). Indeed, in a very strict sense, the iterative map does not have a uniform solution of the form (3.8), except possibly in the limit $M \rightarrow \infty$. Numerical experiments, however, show that for cases where $\alpha\delta^2/2D$ is large,

Equation (3.8) approximates the solution very well over most of the region, and fails only at a few points in the neighborhood of $m = M$. A better approximation of the fixed point can be calculated as an asymptotic expansion in a small parameter, ϵ , as follows. Suppose

$${}^1u^m = 1 - \epsilon^{M-m}, \quad m = 0, \dots, M, \quad (3.10)$$

so that ${}^1u^m \rightarrow 1$ as $m \rightarrow 0$, for very large M . Substituting Equation (3.10) into Equation (3.7) yields,

$$2(1 - \epsilon)[(1 - \mathcal{A}) + \mathcal{A}(1 - \epsilon)] - 1 + \epsilon^2 = 0, \quad (3.11)$$

where $\mathcal{A} \equiv \alpha\delta^2/2D$. Equation (3.11) can be solved for ϵ ,

$$\epsilon = 1, \quad 1/(2\mathcal{A} + 1). \quad (3.12)$$

The first root again represents the trivial fixed point, while the second root represents the ‘‘almost uniform’’ solution. One should note that the condition ϵ very small, which is necessary for the asymptotic expansion to make sense, is valid when \mathcal{A} is very large. Now we show that with the asymptotic expansion (3.10) and the relation (3.12) between ϵ and \mathcal{A} , the fixed point equations are satisfied to order ϵ^2 for all $1 \leq m < M - 1$. Substituting Equation (3.10) into Equation (3.6) yields

$$\mathcal{R}^m = 1 - \epsilon^{M-m-1} - 2(1 - \epsilon^{M-m}) (1 - \mathcal{A}\epsilon^{M-m}) + 1 - \epsilon^{M-m+1},$$

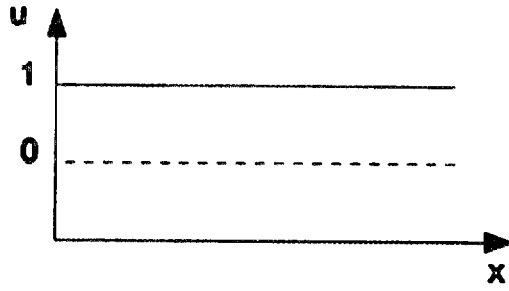
where \mathcal{R}^m is the residue for the m th equation. Eliminating \mathcal{A} using the second root of Equation (3.11) yields

$$\mathcal{R}^m = \epsilon^{M-m}(1 - \epsilon)(1 - \epsilon^{M-m-1}) = O(\epsilon^{M-m}), \quad m = 1, \dots, M - 2. \quad (3.13)$$

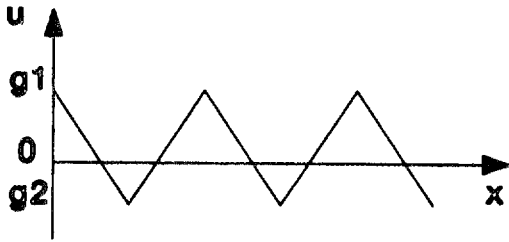
Analogously, the residue for the boundary condition at $m = 0$, Equation (3.5), is $\mathcal{R}^0 = O(\epsilon^{M-1})$. Therefore, for all cases where $M \geq 3$ (which is necessary for the discrete-variable approximation of the diffusion term), all the fixed point equations are satisfied by Equations (3.10) and (3.12) up to order two, at least, in the expansion parameter ϵ . This analysis also shows that the previously^{12,13} employed approximation, Equation (3.9), is approached in the limits $\epsilon \rightarrow 0$ or $M \rightarrow \infty$, and $m < M$.

Fixed points that are not uniform in space can also be found. For example, consider the class of oscillatory solutions with wavelength, λ , equal to 2δ (see Figure 2.b),

$$g_1 \equiv {}^1u^{m-1} = {}^1u^{m+1}, \quad g_2 \equiv {}^1u^m = {}^1u^{m+2}, \quad m > 0, \quad (3.14)$$



a. uniform solutions, $\lambda = \delta$, for $\mathcal{A} > 0$

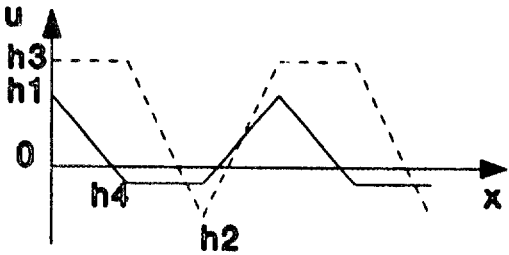


b. oscillatory solutions

$\lambda = 2\delta$, for $\mathcal{A} > 2$

$$g_1 \equiv [\mathcal{A} - 2 + \sqrt{\mathcal{A}^2 - 4}]/2\mathcal{A} > 0,$$

$$g_2 \equiv [\mathcal{A} - 2 - \sqrt{\mathcal{A}^2 - 4}]/2\mathcal{A} < 0.$$



c. oscillatory solutions

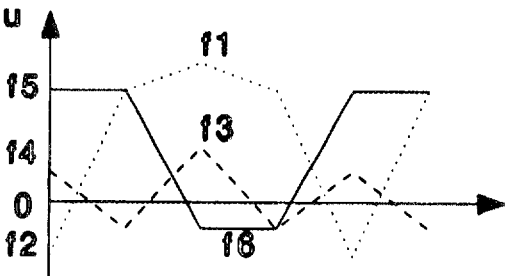
$\lambda = 3\delta$, for $\mathcal{A} > \sqrt{2}$

$$\bar{h}_1 \equiv [\mathcal{A} - 2 + \sqrt{\mathcal{A}^2 - 2}]/2\mathcal{A},$$

$$\bar{h}_2 \equiv [\mathcal{A} - 2 - \sqrt{\mathcal{A}^2 - 2}]/2\mathcal{A} < 0,$$

$$\bar{h}_3 \equiv [\mathcal{A} - 1 + \sqrt{\mathcal{A}^2 - 2}]/2\mathcal{A} > 0,$$

$$\bar{h}_4 \equiv [\mathcal{A} - 1 - \sqrt{\mathcal{A}^2 - 2}]/2\mathcal{A}.$$



d. oscillatory solutions $\lambda = 4\delta$

$$f_1 \equiv [\mathcal{A} - 1 + \sqrt{\mathcal{A}^2 - 1 + 2\sqrt{\mathcal{A}^2 - 1}}]/2\mathcal{A} > 0, \mathcal{A} > 1,$$

$$f_2 \equiv [\mathcal{A} - 1 - \sqrt{\mathcal{A}^2 - 1 + 2\sqrt{\mathcal{A}^2 - 1}}]/2\mathcal{A} < 0, \mathcal{A} > 1,$$

$$f_3 \equiv [\mathcal{A} - 1 + \sqrt{\mathcal{A}^2 - 1 - 2\sqrt{\mathcal{A}^2 - 1}}]/2\mathcal{A} > 0, \mathcal{A} > \sqrt{5},$$

$$f_4 \equiv [\mathcal{A} - 1 - \sqrt{\mathcal{A}^2 - 1 - 2\sqrt{\mathcal{A}^2 - 1}}]/2\mathcal{A} > 0, \mathcal{A} > \sqrt{5},$$

$$f_5 \equiv [\mathcal{A} - 1 + \sqrt{\mathcal{A}^2 - 1}]/2\mathcal{A} > 0, \mathcal{A} > 0,$$

$$f_6 \equiv [\mathcal{A} - 1 - \sqrt{\mathcal{A}^2 - 1}]/2\mathcal{A} < 0, \mathcal{A} > 0.$$

Figure 2. Classes of fixed point solutions to the nonconvective one-dimensional case ignoring the effect of the boundary condition at $x = L$, $m = M$.

where we will ignore the effect of the boundary condition at $m = M$. Substituting Equations (3.14) into Equation (3.6) yields

$$\begin{aligned} g_1 &= 2g_2[(1 - \mathcal{A}) + \mathcal{A}g_2] - g_1, \\ g_2 &= 2g_1[(1 - \mathcal{A}) + \mathcal{A}g_1] - g_2, \end{aligned} \quad (3.15)$$

which can be solved simultaneously for g_1 and g_2 , yielding the trivial and uniform solutions as before, as well as the two new roots,

$$g_1 = \frac{(\mathcal{A} - 2) \pm \sqrt{\mathcal{A}^2 - 4}}{2\mathcal{A}}, \quad g_2 = \frac{(\mathcal{A} - 2) \mp \sqrt{\mathcal{A}^2 - 4}}{2\mathcal{A}}. \quad (3.16)$$

Hence, the spatially oscillatory fixed points (3.14) exist only for $\mathcal{A} > 2$, and even then always produce a negative density, i.e., either $g_1 < 0$ or $g_2 < 0$ (see Figure 2.b). Even though such fixed points have no physical significance, they are valid solutions from the mathematical point of view, as they can be achieved asymptotically from some initial conditions that may lie within their basins of attraction. In the limit $\mathcal{A} \rightarrow 2$, g_1 and $g_2 \rightarrow 0$, so that the $\lambda = 2\delta$ oscillatory solution can be considered as bifurcated from the trivial fixed point as shown in Figure 3. In the limit $\mathcal{A} \rightarrow \infty$, $g_1 \rightarrow 1$ and $g_2 \rightarrow 0$ i.e., a steady state solution that oscillates in space between the two uniform-solution fixed points.

Another class of spatially oscillatory fixed points is the $\lambda = 3\delta$ solutions. Repeating the same process as above, one obtains three quadratic equations which have eight solutions. These equations were solved analytically using the symbolic manipulator MACSYMA.¹⁴⁾ Two of the eight solutions are the trivial and uniform fixed points. Hence, this class contains six fixed points, summarized in Table I, and schematically depicted in Figure 2.c, which are truly of wavelength 3δ . The behavior of this fixed point components, h_1 , h_2 , h_3 , and h_4 , as a function of parameter \mathcal{A} is shown in the bifurcation diagram Figure 3. The $\lambda = 3\delta$ fixed points exist only for $\mathcal{A} > \sqrt{2}$, and they differ from the $\lambda = 2\delta$ fixed points in that as $\mathcal{A} \rightarrow \sqrt{2}$, h_1 and $h_2 \rightarrow (1/2 - 1/\sqrt{2})$ while h_3 and $h_4 \rightarrow (1/2 - 1/2\sqrt{2})$. That is, the $\lambda = 3\delta$ solutions do not bifurcate from either one of the uniform fixed points as did the $\lambda = 2\delta$ fixed points. The $\lambda = 3\delta$ fixed points are similar to the $\lambda = 2\delta$ fixed points, however, in that for $i = 1, \dots, 4$, $h_i \rightarrow$ the uniform fixed points 0 and 1 as $\mathcal{A} \rightarrow \infty$, and in that the oscillations always involve non-physical negative densities. This is clearly the case because $h_1 h_4 \leq 0$ and $h_2 h_3 \leq 0$ for all values of \mathcal{A} .

Of course, one can consider longer wavelengths indefinitely, since we have neglected the boundary conditions. As a last example, we calculated the $\lambda = 4\delta$ fixed points using MACSYMA¹⁴⁾ and the results are summarized in Figure 2.d, Table II, and Figure 4. For this case, there is a total of 16 fixed points, four of which are the two uniform fixed points, and the two $\lambda = 2\delta$ fixed points, leaving twelve truly $\lambda = 4\delta$ oscillatory solutions. These share two features with the above fixed points: each includes a negative, physically unacceptable density, and for $\mathcal{A} \rightarrow \infty$, $i = 1, \dots, 6$, $f_i \rightarrow 0$ or 1 as shown in Figure 4. Also, four fixed points, the (f_3, f_6, f_4, f_6) sequence, exist only for $\mathcal{A} \geq \sqrt{5}$, and do not bifurcate from either one of the uniform fixed points, 0 or 1. Rather, $f_3(\mathcal{A})$ and $f_4(\mathcal{A}) \rightarrow g_1(\mathcal{A})$ as $\mathcal{A} \rightarrow \sqrt{5}$, so that this member of the $\lambda = 4\delta$ class actually bifurcates from the positive branch of the $\lambda = 2\delta$ class as shown in Figure 5.

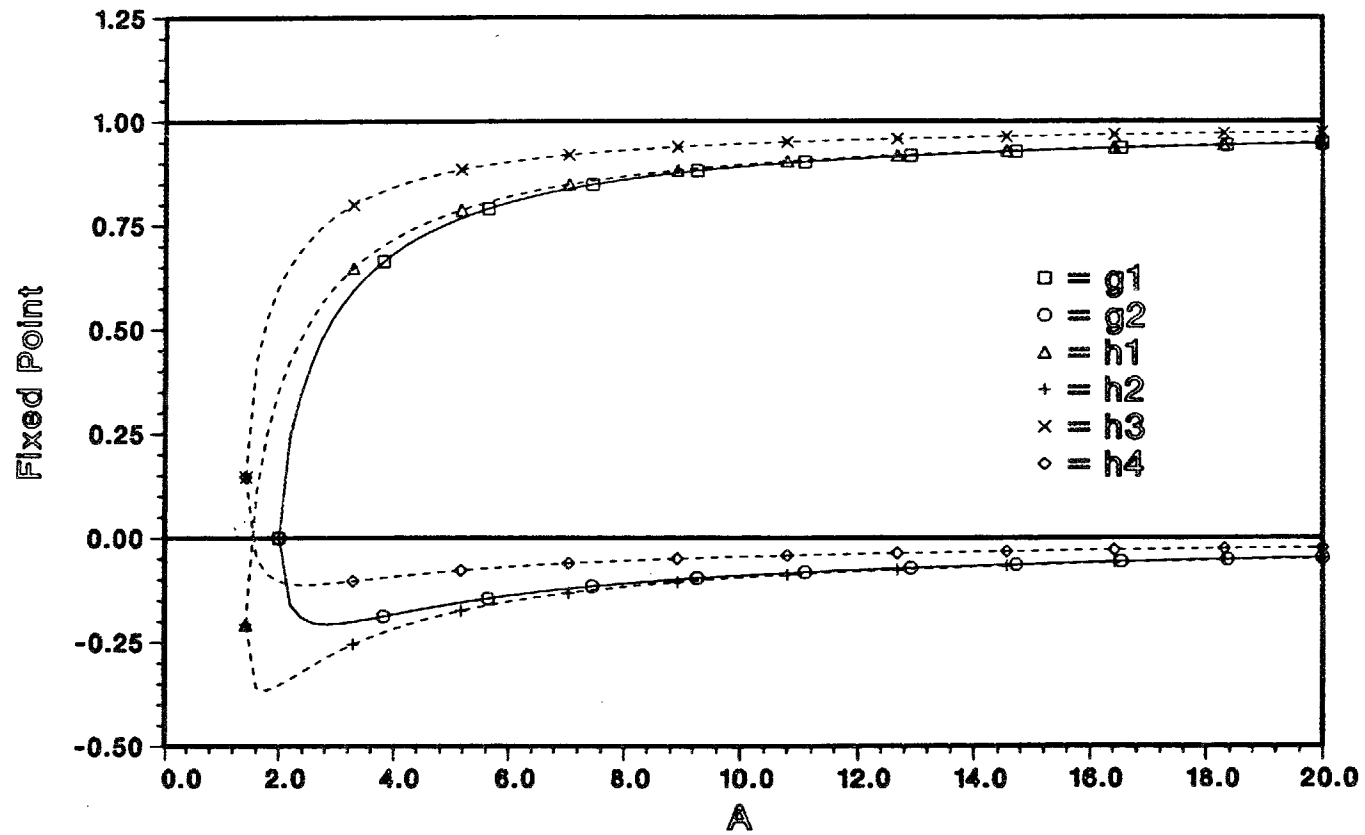


Figure 3. Bifurcation diagram for the $\lambda = 26$ fixed points (solid line) and the $\lambda = 36$ fixed points (dashed line).

Table I.

Members of the Class of Spatially Oscillatory
Fixed Points with Wavelength $\lambda = 3\delta$

1_u^{m-1}	1_u^m	1_u^{m+1}
h_1	h_4	h_4
h_4	h_1	h_4
h_4	h_4	h_1
h_2	h_3	h_3
h_3	h_2	h_3
h_3	h_3	h_2

Table II.

Members of the Class of Spatially Oscillatory
Fixed Points with Wavelength $\lambda = 4\delta$

1_u^{m-1}	1_u^m	1_u^{m+1}	1_u^{m+2}
f_4	f_6	f_3	f_6
f_6	f_3	f_6	f_4
f_3	f_6	f_4	f_6
f_6	f_4	f_6	f_3
f_1	f_5	f_2	f_5
f_5	f_2	f_5	f_1
f_2	f_5	f_1	f_5
f_5	f_1	f_5	f_2
f_5	f_5	f_6	f_6
f_5	f_6	f_6	f_5
f_6	f_6	f_5	f_5
f_6	f_5	f_5	f_6

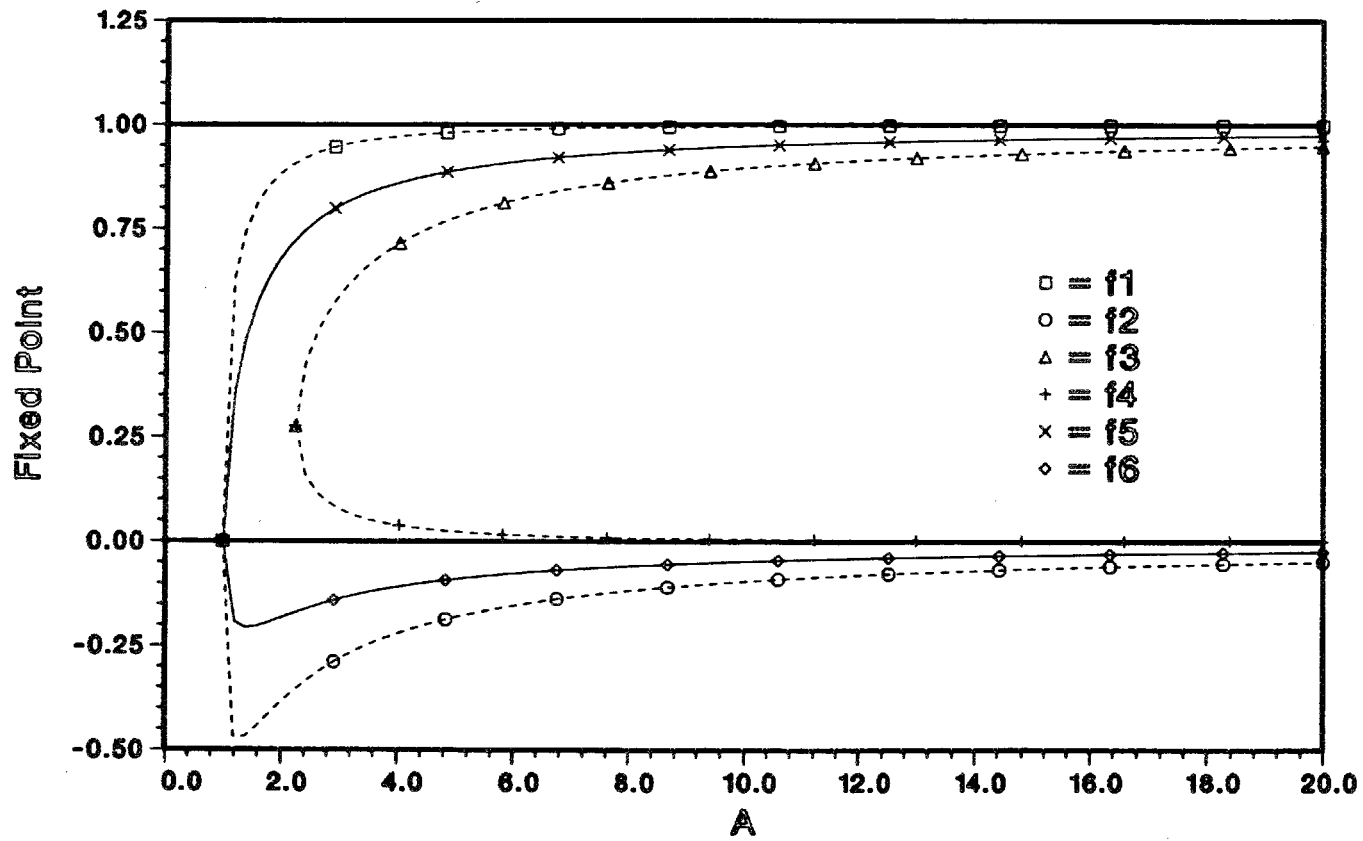


Figure 4. Bifurcation diagram for the $\lambda = 4\delta$ fixed points.

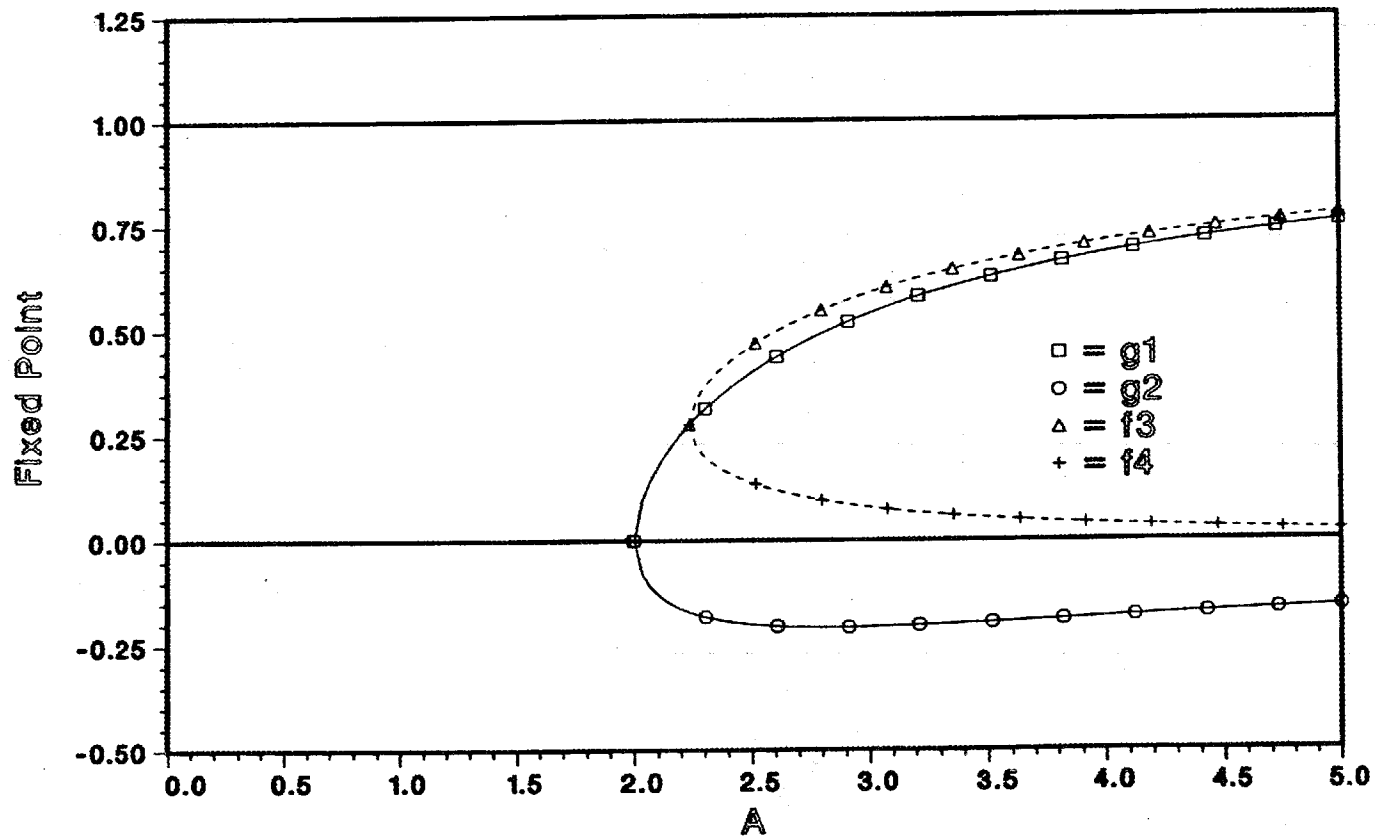


Figure 5. Bifurcation of one $\lambda = 4\delta$ fixed point, the (f_3, f_6, f_4, f_6) sequence from the positive branch of the $\lambda = 2\delta$ fixed point.

The results presented here on fixed points for the one species map have concentrated on the actual calculation of their values, without really considering the two important questions of stability and the effect of the boundary conditions. Importance of these two questions follows from their impact on the observability of the oscillatory solutions. The procedure applied to the uniform solutions to take into account the effect of the boundary conditions may be extended to oscillatory fixed points as well. Initial indications are, however, that oscillatory solutions which yield negative densities are unstable and result in arbitrarily small densities that cause underflow errors on the computer. In this case, these solutions may still be useful in establishing a count for all 2^M fixed points.

3.2 PERIODIC SOLUTIONS

A periodic solution of the iterative map (3.3) exists if there is some integer $\nu > 0$ such that

$${}^\nu u^m \equiv u^{n+\nu, m} = u^{n, m}, \quad m = 0, \dots, M, \quad n \geq 0. \quad (3.17)$$

In this case, ${}^\nu u^m$ is called a period- ν solution of the map. Clearly, ${}^1 u^m$, the period-one solution is a fixed point as defined by Equation (3.4). In previous studies of this iterative map,^{12,13} the dynamics of ${}^\nu u^0$ only was considered, and period-2 and period-4, as well as chaotic patterns for this single quantity were obtained. These results had some unexpected and unexplained features, such as the discontinuities and “blips” in the amplitude of ${}^2 u^0$ as a function of the parameter $b \equiv (D\tau/\delta^2)$.^{12,13} We will show here that these are due to the evolution of the particular initial condition used in these studies^{12,13} to two different solution branches, both of the period-2 class.

Now, we derive the equations for the period-2 class of solutions. For $n = n + 1$, Equation (3.3) becomes

$$\begin{aligned} u^{n+2, m} &= u^{n+1, m} + \mathcal{K}(u^{n+1, m+1} - 2u^{n+1, m} + u^{n+1, m-1}) \\ &\quad + \zeta u^{n+1, m}(1 - u^{n+1, m}), \quad 0 < m < M, \\ u^{n+2, M} &= 0, \\ u^{n+2, 0} &= u^{n+1, 0} + 2\mathcal{K}(u^{n+1, 1} - u^{n+1, 0}) + \zeta u^{n+1, 0}(1 - u^{n+1, 0}), \end{aligned} \quad (3.18)$$

where we defined the constant quantities $\mathcal{K} \equiv \tau D/\delta^2$, $\zeta \equiv \tau\alpha$. Replacing the LHSs of Equations (3.18) using Equation (3.17), and eliminating the $(n+1)$ -level variables on the RHSs in terms of the n -level variables using Equation (3.3), we obtain,¹⁴

$$\begin{aligned} {}^2 u^{n, m} &= -\zeta^3 ({}^2 u^{n, m})^4 + 2\zeta^2 (\zeta - 2\mathcal{K} + 1) ({}^2 u^{n, m})^3 \\ &\quad + [2\mathcal{K}\zeta^2 ({}^2 u^{n, m+1} + {}^2 u^{n, m-1}) - \zeta(\zeta - 2\mathcal{K} + 1)(\zeta - 2\mathcal{K} + 2)] ({}^2 u^{n, m})^2 \\ &\quad + [2\mathcal{K}^2 - s\mathcal{K}\zeta(\zeta - 2\mathcal{K} + 1)({}^2 u^{n, m+1} + {}^2 u^{n, m-1}) + (\zeta - 2\mathcal{K} + 1)^2] {}^2 u^{n, m} \\ &\quad - \zeta\mathcal{K}(\mathcal{K} + 1)[({}^2 u^{n, m+1})^2 + ({}^2 u^{n, m-1})^2] + 2\mathcal{K}(\zeta - 2\mathcal{K} + 1)[{}^2 u^{n, m+1} + {}^2 u^{n, m-1}] \\ &\quad - 2\zeta\mathcal{K}^2 {}^2 u^{n, m+1} {}^2 u^{n, m-1} + \mathcal{K}^2 ({}^2 u^{n, m+2} + {}^2 u^{n, m-2}), \quad m \geq 2, \end{aligned} \quad (3.19a)$$

$$\begin{aligned}
{}^2u^{n,0} = & -\zeta^3({}^2u^{n,0})^4 + 2\zeta^2(\zeta - 2\mathcal{K} + 1)({}^2u^{n,0})^3 \\
& + [4\mathcal{K}\zeta^2({}^2u^{n,1} - \zeta(\zeta - 2\mathcal{K} + 1)(\zeta - 2\mathcal{K} + 2))]({}^2u^{n,0})^2 \\
& + [2\mathcal{K}^2 - 4\mathcal{K}\zeta(\zeta - 2\mathcal{K} + 1)({}^2u^{n,1} + (\zeta - 2\mathcal{K} + 1)^2)]({}^2u^{n,0}) \\
& - 2\mathcal{K}\zeta(2\mathcal{K} + 1)({}^2u^{n,1})^2 + 4\mathcal{K}(\zeta - 2\mathcal{K} + 1)({}^2u^{n,1}) + 2\mathcal{K}^2({}^2u^{n,2}),
\end{aligned} \tag{3.19b}$$

and

$$\begin{aligned}
{}^2u^{n,1} = & -\zeta^3({}^2u^{n,1})^4 + 2\zeta^2(\zeta - 2\mathcal{K} + 1)({}^2u^{n,1})^3 \\
& + [2\mathcal{K}\zeta^2({}^2u^{n,2} + {}^2u^{n,0}) - \zeta(\zeta - 2\mathcal{K} + 1)(\zeta - 2\mathcal{K} + 2)]({}^2u^{n,1})^2 \\
& + [3\mathcal{K}^2 - 2\mathcal{K}\zeta(\zeta - 2\mathcal{K} + 1)({}^2u^{n,2} + {}^2u^{n,0}) + (\zeta - 2\mathcal{K} + 1)^2]({}^2u^{n,1}) \\
& - \mathcal{K}\zeta(\mathcal{K} + 1)[({}^2u^{n,2})^2 + ({}^2u^{n,0})^2] + 2\mathcal{K}(\zeta - 2\mathcal{K} + 1)[{}^2u^{n,2} + {}^2u^{n,0}] \\
& - 2\zeta\mathcal{K}^2({}^2u^{n,2}({}^2u^{n,0}) + \mathcal{K}^2({}^2u^{n,3}).
\end{aligned} \tag{3.19c}$$

For M computational cells, Equations (3.19) represent a set of M fourth-order algebraic equations whose real solutions are period-2 solutions of the iterative maps. Solving this system analytically for any reasonable value of M is practically impossible. Therefore, as was done previously with the fixed points, we rely on numerical experiments to specify some classes of periodic solutions which simplify Equations (3.19) significantly to the point of making them solvable analytically, at least for ${}^2u^{n,0}$.

By observing the behavior of $u^{n,m}$, for several values of the parameters in the problem, as a function of the iteration index n , for all mesh points m , one notices that the solution consists of a spatially oscillatory component with an almost fixed amplitude. The peaks and troughs of this component of the solution interchange with n giving rise to the periodic nature of the solution. In addition, there is a uniform component of the solution; one or more neighboring points having the same magnitude at each n . The oscillatory and uniform components of the solution are interspersed along the x-axis as depicted in Figure 6. The particular pattern, i.e., the position and width of the oscillatory and uniform components, that an initial point converges to depends on that initial point as well as the parameters in the problem. Hence, we immediately identify two classes of period-2 solutions which are easily dissociated from the large system of Equations (3.19) and are solved for ${}^2u^0$ as a function of \mathcal{K} and ζ .

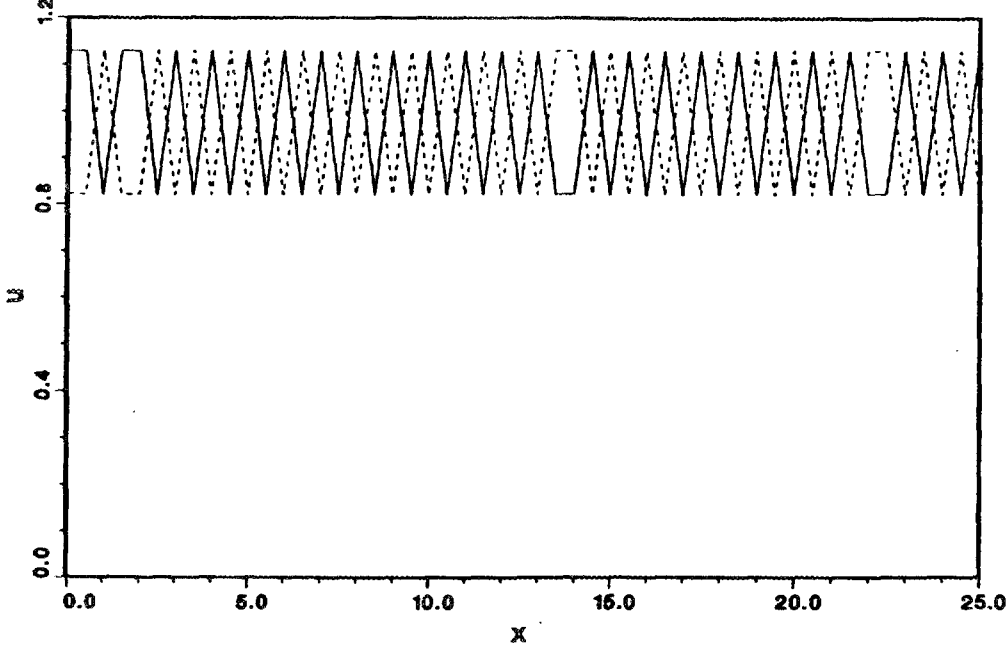


Figure 6. Sample period-2 solution for $0 \leq m \leq 50$, $\alpha = 16.8$, $D = .002$, and initial condition $u^{0,0} = 3.1/3$, $u^{0,m} = 0$, $m > 0$.

The first class of period-2 solutions is characterized by the relations

$$\begin{aligned} {}^2u_1^0 &\equiv u^{n,0} = u^{n,1} = u^{n+2,0} = u^{n+2,1}, \\ {}^2u_2^0 &\equiv u^{n+1,0} = u^{n+1,1} \neq {}^2u_1^0, \quad n \geq 0. \end{aligned} \quad (3.20)$$

Substituting these relations into the last equation in (3-18) yields

$$\begin{aligned} {}^2u_1^0 &= {}^2u_2^0 \{1 + \zeta(1 - {}^2u_2^0)\}, \\ {}^2u_2^0 &= {}^2u_1^0 \{1 + \zeta(1 - {}^2u_1^0)\}. \end{aligned} \quad (3.21)$$

Solving these two equations simultaneously yields the two fixed points ${}^1u^0 = 0$ and 1 in addition to the two period-2 values of u , at $m = 0$,

$${}^2u^0 = \left[\zeta + 2 \pm \sqrt{\zeta^2 - 4} \right] / 2\zeta. \quad (3.22)$$

Hence, periodic solutions in this class have a magnitude that is independent of \mathcal{K} , and exist only when the value of parameter $\zeta > 2$. For $\zeta = 2$, the two solutions ${}^2u^0$ coincide with the fixed point ${}^1u^0 = 1$, so that this period-2 solution seems to bifurcate from the uniform steady-state solution at $\zeta = 2$ for any \mathcal{K} .

The second class of period-2 solutions is characterized by the relations

$$\begin{aligned}
{}^2u_1^0 &\equiv u^{n,0} = u^{n+1,1} = u^{n+2,0} = u^{n+3,1}, \\
{}^2u_2^0 &\equiv u^{n+1,0} = u^{n,1} \neq {}^2u_1^0, \quad n \geq 0.
\end{aligned} \tag{3.23}$$

Substituting these solutions into the last equation in (3.18) yields

$$\begin{aligned}
{}^2u_1^0 &= {}^2u_2^0 \{1 - 2\mathcal{K} + \zeta(1 - {}^2u_2^0)\} + 2\mathcal{K} {}^2u_1^0, \\
{}^2u_2^0 &= {}^2u_1^0 \{1 - 2\mathcal{K} + \zeta(1 - {}^2u_1^0)\} + 2\mathcal{K} {}^2u_2^0.
\end{aligned} \tag{3.24}$$

Again, solving these two equations simultaneously produces the two fixed points ${}^1u^0 = 0$ and 1 in addition to the two period-2 values of u at $m = 0$,

$${}^2u^0 = \left[\zeta - 4\mathcal{K} + 2 \pm \sqrt{\zeta^2 - 16\mathcal{K}^2 + 16\mathcal{K} - 4} \right] / 2\zeta. \tag{3.25}$$

The magnitude of the periodic solutions in this class depends on both ζ and \mathcal{K} , in such a way that period-2 solutions of this type exist only in the shaded region of the (\mathcal{K}, ζ) plane shown in Figure 7, where we have also enforced the physical constraints $\mathcal{K}, \zeta \geq 0$. This figure clearly indicates that for any physical value of $\mathcal{K}(\zeta)$, there are infinitely many values of $\zeta(\mathcal{K})$ at which the period-2 second class solution exists, respectively. The magnitude of ${}^2u^0$ on the boundary of the period-2 region is 0 on the solid line portion, and 1 on the dashed portion, indicating that period-2 second class solutions bifurcate from the trivial (uniform) fixed point solution on the solid (dashed) boundary in the (\mathcal{K}, ζ) plane. Figure 8 shows ${}^2u^0$ as a function of ζ for several values of \mathcal{K} ; the dashed curve represents the class 1 solution, Equation (3.22), for all \mathcal{K} , while the solid curves represent the class 2 solutions, Equation (3.25), for the indicated values of \mathcal{K} . Note that at $\mathcal{K} = 0$, the period-2 class 2 solution coincides with the class 1 solution. On the other hand, Figure 9 presents second class ${}^2u^0$ as a function of \mathcal{K} for several values of ζ ; first class ${}^2u^0$ is not a function of \mathcal{K} , therefore, it is not shown. The closed curves indicate that solutions in this class do not exist for indefinitely large values of \mathcal{K} , as also clear from Figure 7; rather, for each ζ , this solution exists only for a finite range of \mathcal{K} . Two additional interesting facts immediately follow from Figure 9. First, for $\zeta < 2$, the bifurcation of the fixed point into the periodic solution occurs at a positive value of \mathcal{K} , so that both steady-state and periodic solutions can be observed for physical values of $\mathcal{K} \geq 0$. In contrast, for all $\zeta > 2$, the bifurcation point occurs at $\mathcal{K} < 0$, so that only periodic solutions can be observed for physical values of $\mathcal{K} \geq 0$; this type of behavior has been computed numerically in Refs. 12 and 13. Second, for values of $\mathcal{K} > .5$, one of the period-2 points is negative, while for all $\mathcal{K} < .5$, both points for any ζ are positive. This behavior was not observed in previous studies^{12,13} because period doubling bifurcations, chaos, and divergence occurred at much smaller values of \mathcal{K} than 0.5.

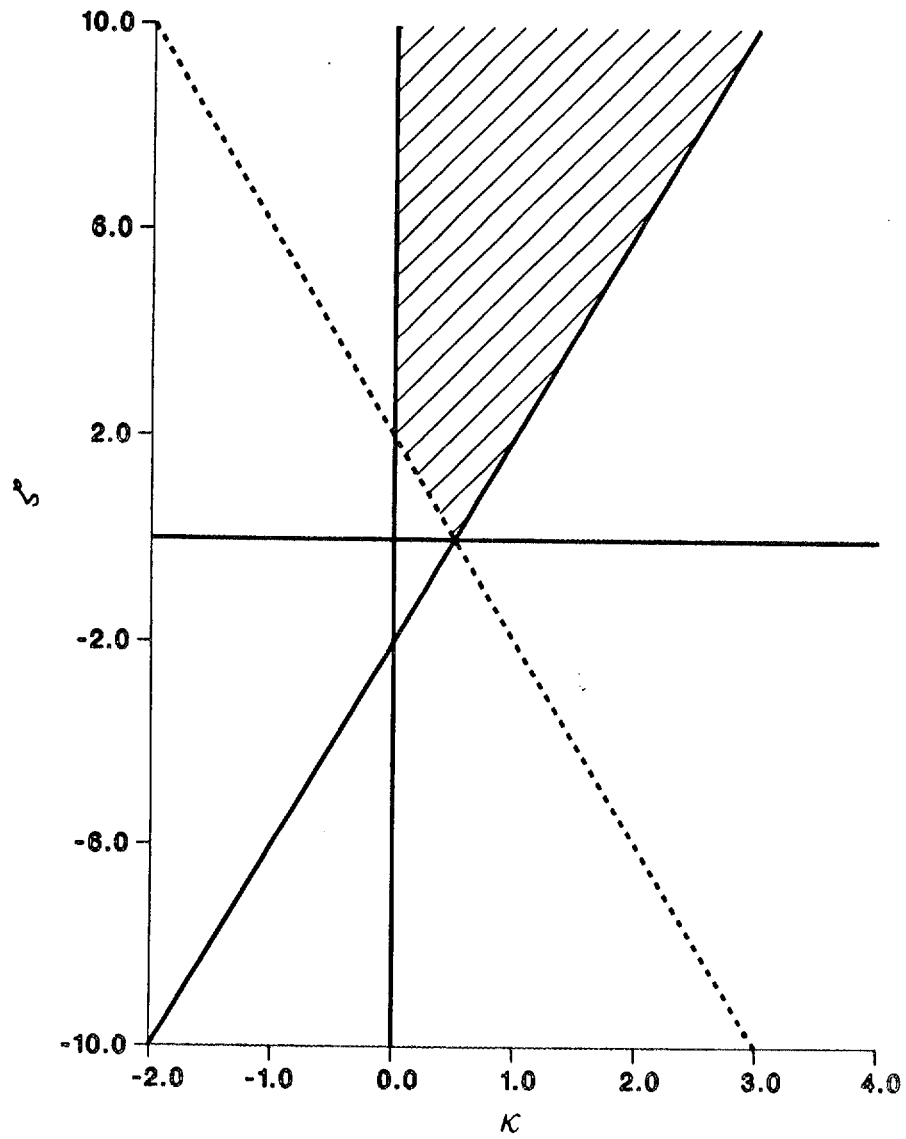


Figure 7. Region of existence of the period-2 second class solution in the (K, ζ) plane. The part of this region that is physically acceptable, $K, \zeta \geq 0$, is hatched.

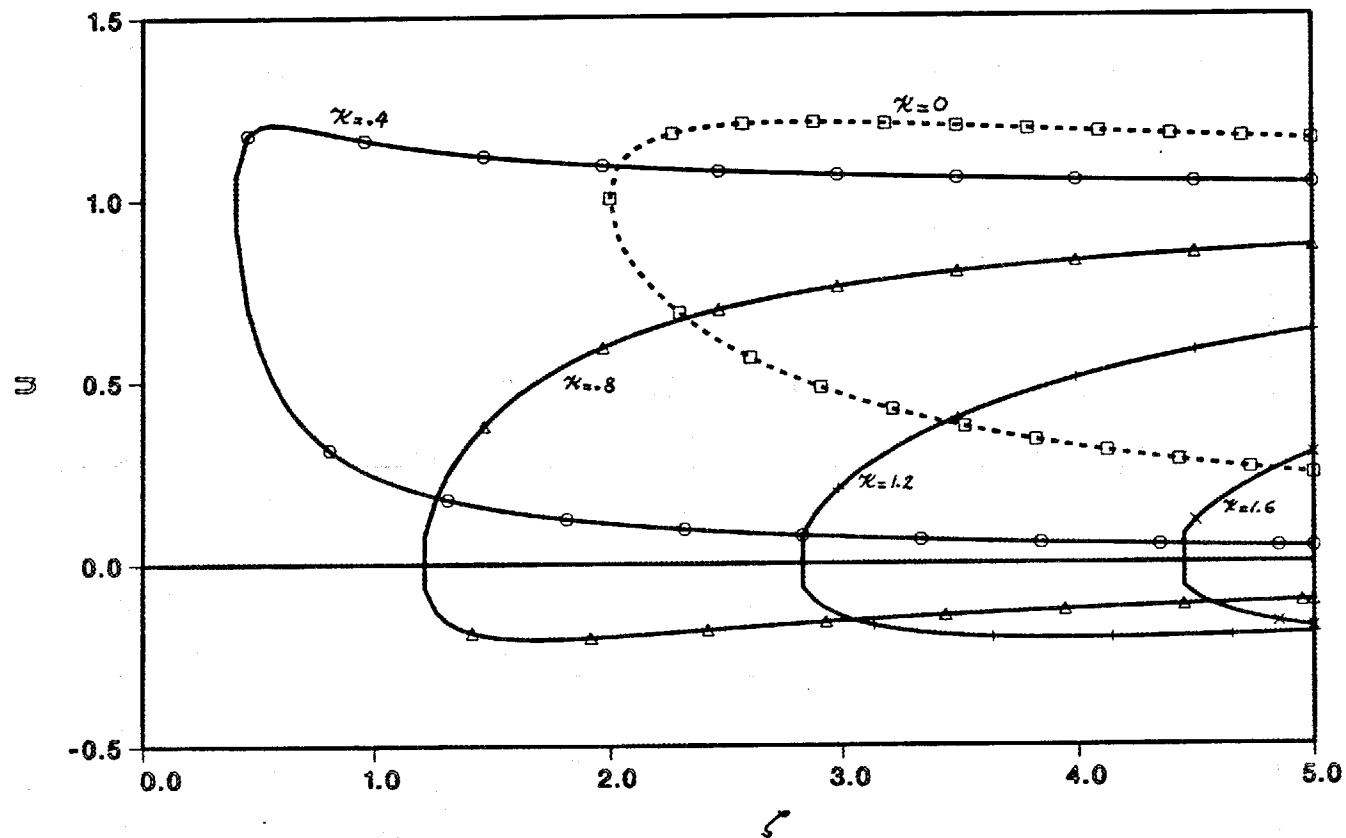


Figure 8. Bifurcation diagram for period-2 first class (dashed) and second class (solid) solutions as a function of ζ for various values of κ

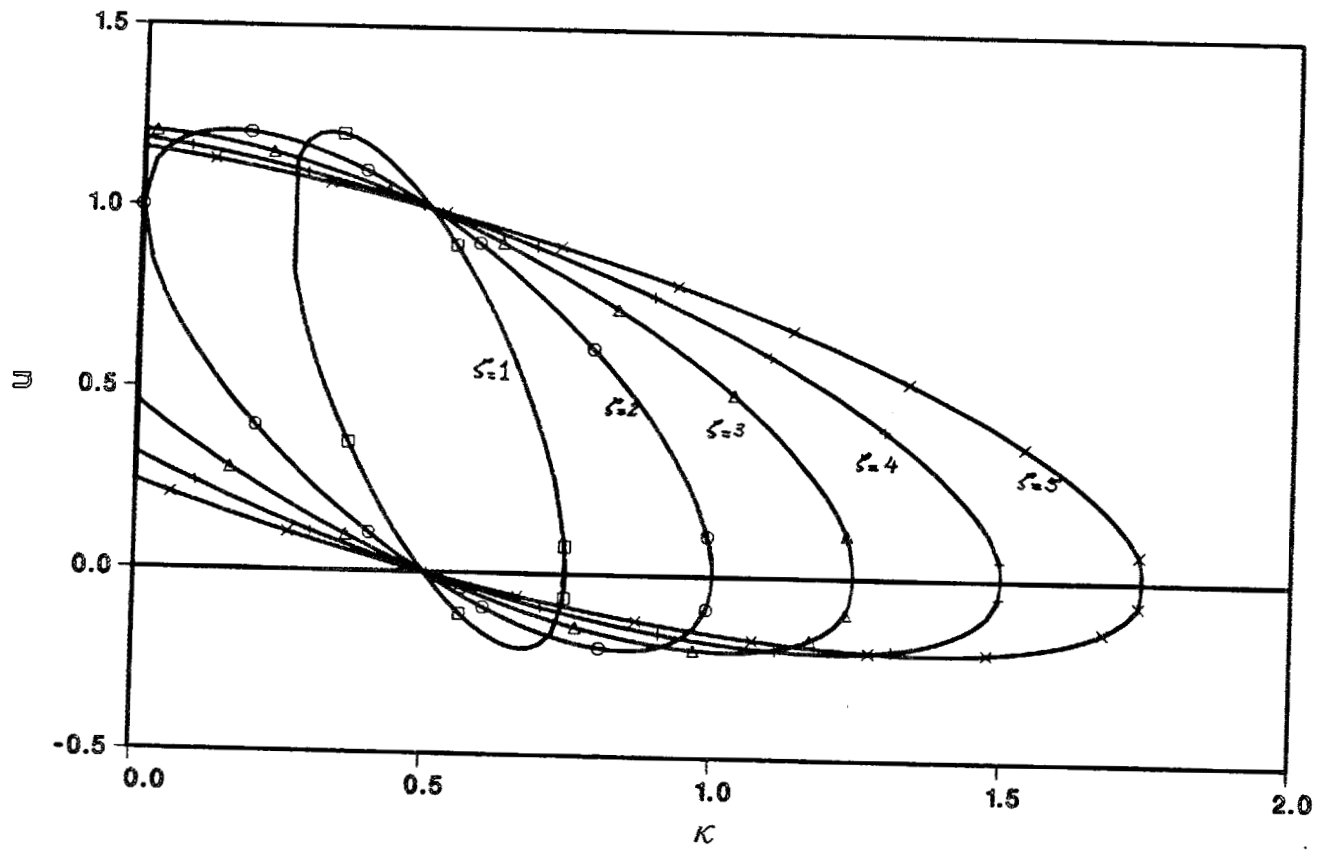


Figure 9. Bifurcation diagram for period-2 second class solution as a function of K for various values of ζ .

The analytic investigation of periodic solutions that is presented in this section is based completely on equality properties that are experimentally (i.e., computationally) observed which enabled us to dissociate two equations from the full system, Equations (3.19), whose simultaneous solution specifies certain classes of period-2 solutions. Obviously, there are many more classes of period-2 solutions satisfying other more complicated symmetry conditions, and resulting in larger systems of coupled algebraic equations, whose analytic solution is more difficult. However, by comparing the period-2 solution branches obtained here with those reported in Ref. 12, one finds that the initial condition used in that work results in asymptotic convergence to period-2 solutions of the second class in the majority of the parameter ranges considered. However, discontinuities and “blips”^{12,13)} appearing, and not explained, in the bifurcation diagram actually correspond to asymptotic period-2 solutions that do not belong to either class considered here. These classes of period-2 solutions, as well as period-4 solutions may be studied in the future with the aid of the symbolic manipulator MACSYMA.¹⁴⁾ Plots of the asymptotic state for $0 \leq x \leq 10$ at n and $n + 1$ for parameter values corresponding to these discontinuities^{12,13)} are shown in Figure 10 clearly justifying the above statement.

3.3 NON-VANISHING CONVECTION

With the present understanding of the non-convective case, now we turn our attention to the case of non-zero convection. Obviously, the effect of convection on the time-space evolution of the density of one species is that it superimposes a bulk motion of that species on its diffusive motion. This indeed has been observed in numerical experiments we performed using values of $c = .25, .5,$ and $.75$. In some sense, c represents the speed of propagation of a signal (or density perturbation) in the complete absence of diffusion. Hence, for a battlefield of length L , a signal originating at one end reaches the other end in time $T = L/c$ due to convection alone.

Another important effect of convection is the way it alters the bifurcation diagram. To study this feature, we selected a few cases from the bifurcation diagrams in Ref. 3 which represent all possible steady state and periodic regimes, and calculated their time evolution using the non-zero convection values mentioned above. The nature of the asymptotic regime for each case, as well as for $c = 0$ ¹²⁾ is listed in Table III. The results suggest that convection, in general, appears to increase the effective value of the diffusion coefficient. That is, regimes with non-zero convection at a given value of the diffusion coefficient produce asymptotic regimes of the same nature as those produced with zero convection and a larger value of the diffusion coefficient. Clearly, this is only a rough observation because we did not consider a sufficiently large number of points in parameter space, and because we compared only the general nature of the asymptotic regimes rather than the full temporal evolution. However, it is easy to see from the definitions of \mathcal{D}_{i+}^m , \mathcal{D}_i^m , and \mathcal{D}_{i-}^m , Equations (2.5), that a positive convection results in the values of these parameters larger or equal to their values when $c = 0$, the case of pure diffusion. In other words, for non-zero convection, Eq. (3.2) will have effective diffusion coefficients, the \mathcal{D} 's, that are anisotropic (i.e., $\mathcal{D}_{i+}^m \neq \mathcal{D}_{i-}^m$), and larger in

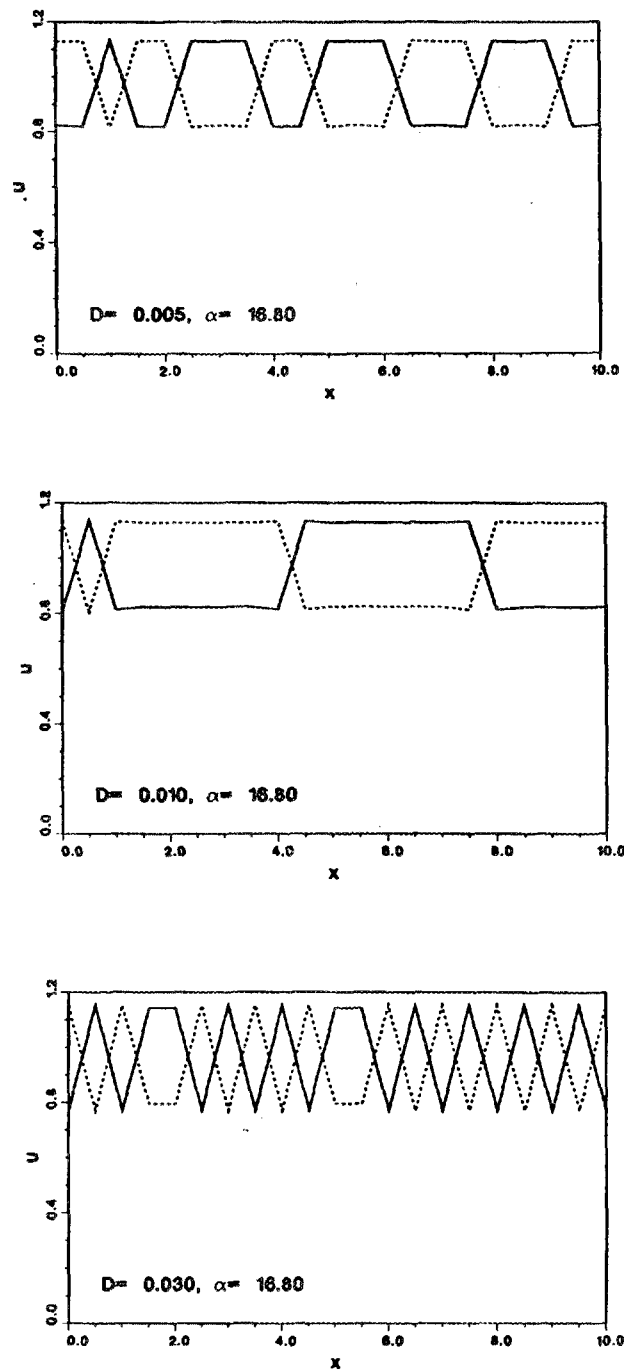


Figure 10. Sample plots of u vs. x at two consecutive time steps, with parameter values corresponding to points surrounding discontinuities in Figure 4 of Ref. 12. These plots clearly show that these discontinuities occur at parameter values that cause a change in the solution class (i.e., the symmetry relations at the left boundary).

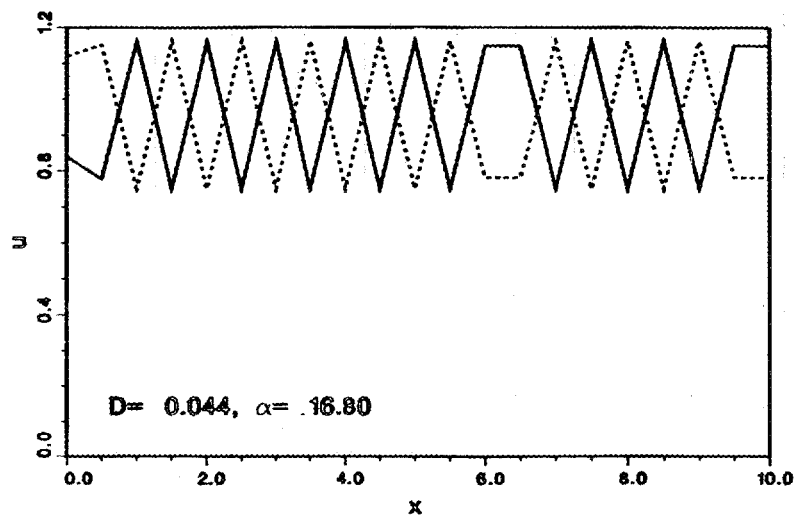
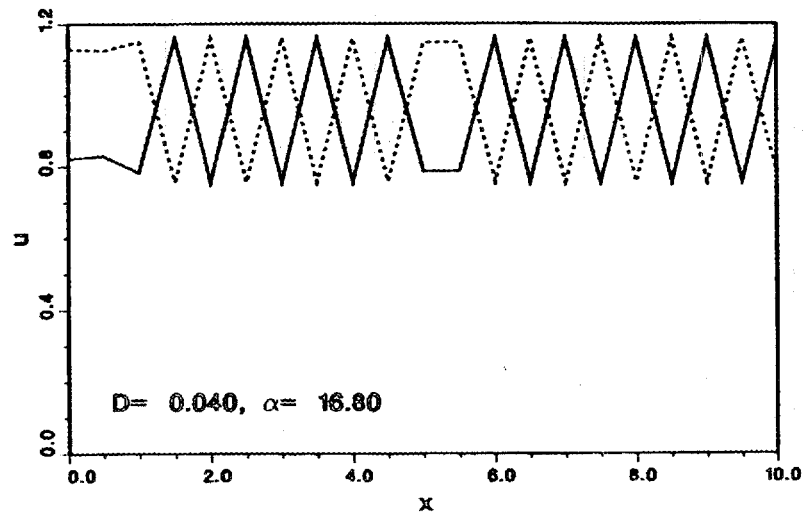
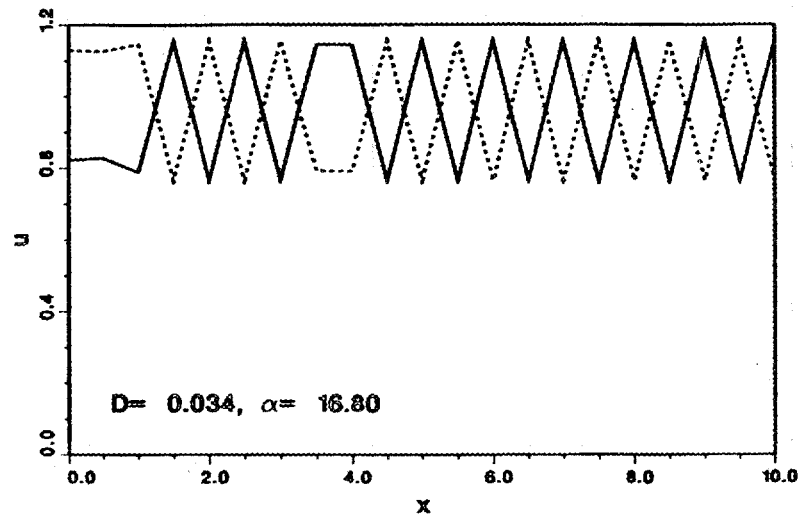


Figure 10. Continued

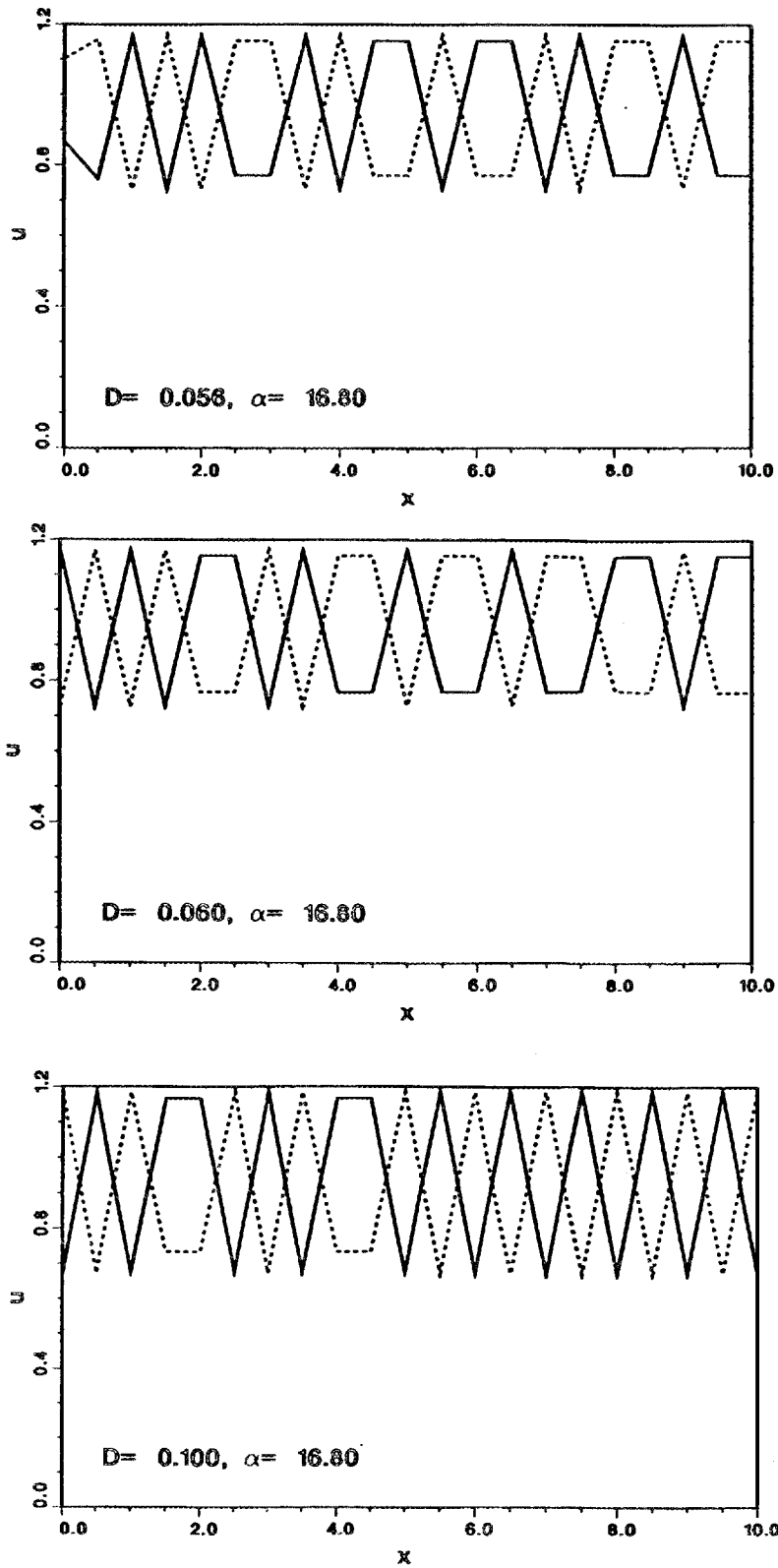


Figure 10. Continued

magnitude than their counterparts in the same equation for $c = 0$. This, at least partially, explains the observations made from the results in Table III. Moreover, these results suggest that the system is structurally stable in the shape of the diffusion coefficient as a function of space. That is, perturbations in $D(x)$ of the non-isotropic type described above in connection with the \mathcal{D} 's, does not change the bifurcation diagram dramatically.

Table III.

Effect of Convection on the Temporal Behavior of
Sample Cases Presented Previously in Refs. 12 and 13

Case	α	D	u_0	$c = 0$ †	$c = .25$	$c = .5$	$c = .75$
1	12	.2	.8333	$p-0^*$	$p-1$	$p-1$	
2	12	.4	.8333	$p-1$	chaotic	chaotic	
3	15.32	.03	.761097	$p-0$	$p-1$	$p-1$	$p-1$
4	15.32	.08	.761097	$p-1$	$p-1$	$p-1$	chaotic
5	16.8	.02	.738096	$p-1$	$p-1$	$p-1$	chaotic
6	16.8	.04	.738096	$p-1$	$p-1$	$p-1$	chaotic
7	16.8	.06	.738096	$p-1$	$p-1$	chaotic	
8	16.8	.08	.738096	$p-1$	$p-1$	chaotic	
9	19.2	.012	.708333	$p-1$	$p-2$		
10	19.2	.03	.708333	$p-1$	chaotic		
11	19.2	.05	.708333	$p-2$	chaotic		
12	19.2	.07	.708333	chaotic	chaotic		

†From Refs. 12 and 13.

* $p - n$ solution has period 2^n ; $p - 0$ is steady state

4. THE DYNAMICS OF INTERACTING TWO-SPECIES SYSTEMS

In this section, we investigate the dynamics of the two-species iterative map, Eq. (2.6), with non-vanishing competitive interaction. Because of the very large amount of data generated in the process of evaluating the evolution of example cases, we equipped our computer program, CMAP1, that performs this function, with animation capability that utilizes DISSPLA library subroutines. This has the advantage of enabling us to visually observe the evolution of a battle for extended periods of time, i.e., large iteration numbers, in full spatial detail. It also has the disadvantage of making it very difficult to report the results in an exhaustive manner; therefore, here we will present the input parameters, discuss the purpose of each calculation, and the specific features of the solution that we believe makes each case interesting.

In order to simulate a battle between two military forces, we consider a battlefield of length $L = 25$ units, divided into 50 computational cells, each of width $\delta = .5$ units. The finite time increment is set to .125 units. The first military force, $u_1^{n,m}$, $n \geq 0$, $0 \leq m \leq 50$, is the defender initially entrenched in one-fifth of the battlefield, $0 \leq m \leq 10$, and moving forward only through the effect of diffusion but no convection, $c_1 = 0$ uniformly. The initial density of the defender is $u_1^{0,m} = U_1$, $0 \leq m \leq 10$, and $u_1^{0,m} = 0$, $10 < m \leq 50$. The second military force, $u_2^{n,m}$, $n \geq 0$, $0 \leq m \leq 50$, is the attacker approaching the defender at a uniform bulk speed of $c_2 \neq 0$ from outside the battlefield so that initially the density of the attacker is $u_2^{0,m} = U_2 \neq 0$, $m = 50$, and $u_2^{0,m} = 0$, $0 \leq m < 50$. With $c_2 < 0$, the attacker moves into the battlefield through the left boundary at L under the effect of both convection and diffusion. The boundary conditions imposed on both species were kept analogous to those used in Refs. 12 and 13; namely,

$$\begin{aligned} du_1/dx &= 0, \quad \text{at } x = 0, \quad u_1(L, t) = 0, \\ u_2(0, t) &= 0, \quad du_2/dx = 0, \quad \text{at } x = L. \end{aligned} \tag{4.1}$$

The volumetric external source \bar{s}_i^m is set equal to zero for both species, relying on the boundary source represented by the boundary conditions to replenish the supply for each force. To simplify the investigation of the possible bifurcations, we reduced the number of independent interaction parameters by assuming the following relations among them,

$$\begin{aligned} \alpha_{iii} &= -\beta_{ii} = \alpha_i, \\ \alpha_{ijj} &= \alpha_{iji} = \alpha_{ij}, \\ \alpha_{ijj} &= 0 = \beta_{ij}, \quad i = 1, 2, \quad j \neq i. \end{aligned} \tag{4.2}$$

At this point, the set of independent parameters that can be adjusted to study the dynamical behavior of this battle model includes, for each species, the uniform magnitude of the diffusion coefficient, D_i , the initial density parameter, U_i , the interaction coefficients, α_i and α_{ij} , and for the attacking force the convective speed, c_2 . In selecting values for these parameters, however, we tried to keep them consistent with values chosen previously at various dynamic regimes for the

one species system as shown in Table III. By choosing $\alpha_{ijj} = 0 = \beta_{ij}$, one force will evolve as it would have in a one-species system in all regions where the other force has a vanishing density. Hence, in the approach stage of a battle preceding engagement of the two forces, they move toward one another in an uncoupled fashion. Only after engagement is the evolution of each force influenced by the existence of the other force.

As a first example, we ran a symmetric (in the two species) low diffusion case, $D_1 = D_2 = .05$, with the attacker approaching at a speed of $c_2 = .75$. We chose $U_1 = U_2 = .8333$, and $\alpha_1 = \alpha_2 = 12$, $\alpha_{12} = \alpha_{21} = 12$. [We noticed that increasing the "enemy" destruction rate, α_{ij} , $i \neq j$, to 15, for example, leads to unbounded solutions.] The noninteractive case for this battle leads to steady state solutions for both species at very large times. The "front" of each species progresses due to diffusion for species 1, and combined diffusion-convection for species 2, unhindered until it reaches the opposite end of the battlefield where it is forced by the boundary condition to stop and reach a steady, almost uniform, distribution asymptotically in the iteration index, or time variable.

The case with interaction was allowed to run for 240 time steps, i.e., 30 time units. Each species moves forward unhindered for 41 time steps, $t = 5.125$, at which time they engage halfway through the battlefield, $x \simeq 12.5$. Progress of both species then is halted for a few time steps then the attacking species overcomes the defender and starts pushing it back very slowly, so that by the end of 80 steps, $t = 10$, the battle front is at $x \sim 11$. Two features that are interesting from the dynamical point of view result from introducing intraspecies interactions. First is the onset of oscillations, both in space and time, in the two species, but which are far more pronounced in the defender. These oscillations are larger near the battle front and get smaller as one moves toward the edges of the battlefield. Second is the appearance of negative densities, which are very small in magnitude and are of oscillatory nature, in spite of the imposed condition $\alpha_{ijj} = 0 = \beta_{ij}$, $i \neq j$. The negative densities for each species occurs immediately outside the battle front for that species, where the density is small to start with and very small losses can be larger than the local density.

As time passes, the attacker continues to push the defender backwards, continuously depleting the latter's total population, so that by the end of 240 time steps, $t = 30$, the defender is back to $x \simeq 6$, close to where it originally started at $t = 0$, down from a maximum at the time of engagement of $x \simeq 12.5$.

As a variation on this battle, we reduced the destruction rate of the defender by the attacking force by one half, i.e., $\alpha_{112} = \alpha_{121} = 6$, thus giving the defender a factor of two advantage in the enemy destruction rate over the attacker. This case was allowed to run for 160 time steps, i.e., until $t = 20$. Of course, the approach stage remained unchanged, and the two species engaged at $x \simeq 12.5$, $t \simeq 5.125$. Then, the defender, species 1, was able to stop the advance of the attacker, species 2, and pushed it back slowly so that at $t = 20$, the battle front occurred at $x \simeq 17$. This behavior, however, should not be confused with enemy pursuit, which may be desirable to include in future models, because here the advance of the defender is of pure diffusive nature. Pursuit, on the other hand, should be based on a deliberate decision at a given point during the progress of the battle to change the convective speed of the species to a nonzero value. The previous remarks on the onset of

oscillations in the densities of the two species, and on the occurrence of negative densities of small magnitude are true here also.

One final variation on this sample battle is an intermediate value of the defender destruction rate, $\alpha_{12} = 9$. Everything else left unchanged this case produced a stalemate, i.e., a nontrivial steady state, whereby the battle front stayed at the same point for many time steps. This result gives an explicit example of the practical usefulness of this research effort. A commander of a friendly military force that is subject to battle with an enemy (attacking or defending) can estimate the necessary improvement in his army's destructive power that will enable him to win the battle. That is, if he is defending, he has to make sure his army can destroy the enemy at a rate larger than $4/3$ the enemy's rate of destroying his force, and vice versa.

At present, a more flexible variant of the program has been developed¹⁵⁾ on which an exhaustive parametric study will be conducted. A parallelized version of the same program is also completed¹⁶⁾ and preliminary tests show a reduction of the CPU time by a factor of 20-25 to less than one second. The full exploitation of these programs and the interpretation of their results will be reported in a future publication.

Acknowledgements

This research has been sponsored by DARPA under contract number 1868-A037-A1 with Martin Marietta Energy Systems, Inc., which is under contract number DE-AC05-84OR21400 with the U.S. Department of Energy.

REFERENCES

1. N. S. Goel, S. C. Meritra, and E. W. Montroll, "On the Volterra and Other Non-Linear Models of Interacting Populations," *Rev. Mod. Phys.* **43**, 231 (1971).
2. Patrick J. Roache, *Computational Fluid Dynamics*, Hermosa Publishers, Albuquerque, New Mexico (1972).
3. F. W. Lanchester, "Aircraft in Warfare: The Dawn of the Fourth Arm—No. V. The Principle of Concentration," *Engineering* **98**, 422 (1914).
4. J. G. Taylor, *Lanchester Models of Warfare*, Vols. 1 and 2, MAS Operation Research Society of America, Virginia, 1983.
5. V. Protopopescu, R. T. Santoro, and J. Dockery, "Combat Modeling with Partial Differential Equations," *European J. Operations Research* **38**, 178 (1989).
6. S. A. Levin, ed., *Studies in Mathematical Biology*, Parts I, II, The Mathematical Association of America, 1978.
7. P. C. Fife, *Mathematical Aspects of Reactions—Diffusion Systems Lecture Notes in Biomathematics*, Vol. 28, Springer Verlag, Berlin, 1979.
8. J. Smoller, *Shock Waves and Reaction Diffusion Equations*, Springer Verlag, New York.
9. E. S. Oran and J. P. Boris, *Numerical Simulation of Reactive Flow*, Elsevier, New York, 1987.
10. C. Cosner, S. Lenhart, and V. Protopopescu, "Parabolic Systems with Nonlinear Competitive Interactions," ORNL/TM-11071, January 1989.
11. S. Lenhart, S. Stojanovic, and V. Protopopescu, "Variational Approach for Competitive Systems with Obstacles," in preparation.
12. A. R. Mitchell and J. C. Bruch, Jr., "A Numerical Study of Chaos in a Reaction-Diffusion Equation," *Numer. Meth. Part. Diff. Eqs.*, **1**, 13 (1985).
13. James J. Wachholz and John C. Bruch, Jr., "An Investigation of Chaos in Reaction-Diffusion Equations," *Numer. Meth. Part. Diff. Eqs.*, **3**, 139 (1987).
14. *VAX UNIX MACSYMA Reference Manual, Version 11*, Symbolics Inc. (1985).
15. S. De Rada and V. Protopopescu, "Two Dimensional Maps with Competitive Interactions," in preparation.
16. S. Antommarchi and Y. Y. Azmy, "A Parallel Algorithm for Solving Time Dependent Diffusion Equations," in preparation.

INTERNAL DISTRIBUTION

- | | |
|-------------------------|---|
| 1. R. G. Alsmiller, Jr. | 19-23. R. T. Santoro |
| 2. B. R. Appleton | 24. EPMD Reports Office |
| 3-7. Y. Y. Azmy | 25-26. Laboratory Records
Department |
| 8. J. M. Barnes | 27. Laboratory Records,
ORNL-RC |
| 9. D. E. Bartine | 28. Document Reference
Section |
| 10. R. M. Davis | 29. Central Research Library |
| 11. C. M. Haaland | 30. ORNL Patent Section |
| 12. D. T. Ingersoll | |
| 13. F. C. Maienschein | |
| 14-18. V. Protopopescu | |

EXTERNAL DISTRIBUTION

31. Dr. L. Auslander, Defense Advanced Research Projects Agency, 1400 Wilson Blvd., Arlington, Virginia 22209
32. Mr. Donald Butts, J6F, Organization of the Joint Chiefs of Staff, The Pentagon, Washington, D.C. 20301-5000
33. COL G. Q. Coe, J6F, Organization of the Joint Chiefs of Staff, The Pentagon, Washington, D.C. 20301-5000
34. J. Dockery, Office of the Joint Chiefs of Staff, J6F, The Pentagon, Washington, D.C. 20301
35. J. J. Dorning, Department of Nuclear Engineering and Engineering Physics, Thornton Hall, University of Virginia, Charlottesville, Virginia 22901
36. R. M. Haralick, Department of Electrical Engineering, University of Washington, Seattle, Washington 98195
37. Petre Rusu, Physics Department, University of Colorado, Campus Box 390, Boulder, Colorado 80309
38. Dr. Ben Wilcox, Defense Advanced Research Projects Agency, 1400 Wilson Blvd., Arlington, Virginia 22209
39. Office of the Assistant Manager for Energy Research and Development, Department of Energy, Oak Ridge Operations, P.O. Box 2001, Oak Ridge, TN 37831
- 40-49. Office of Scientific and Technical Information, P.O. Box 62, Oak Ridge, Tennessee 37830